UNIVERSITY OF CALIFORNIA
RIVERSIDE

Complex Characteristics of Slow Slip Events and Their Influence on Subduction Zone Dynamics Based on Multi-Cycle Simulations

A Dissertation submitted in partial satisfaction
of the requirements for the degree of

Doctor of Philosophy

in

Geological Sciences

by

Harmony Colella

December 2011

Dissertation Committee
Dr. James Dieterich, Chairperson
Dr. Gareth Funning
Dr. Elizabeth Cochran

The Dissertation of Harmony Colella is approved:

Committee Chairperson

University of California, Riverside

Acknowledgements

The completion of this dissertation was only possible because of the support and dedication of my family and colleagues. First, I would like to thank my committee: James Dieterich, Elizabeth Cochran, and Gareth Funning. Elizabeth – You have not only been a mentor and advisor, but also a friend. I have always been able to discuss anything with you. I hope to maintain a professional and personal relationship with you for years to come. Gareth, ah Gareth, without you, I would not have as thick of a skin. While it is sometimes hard to hear, I thank you immensely for your blunt criticism as it has made me a better scientist, teacher, and person. Additionally, without you, the last few months would have been much more difficult, if not impossible. Your support does not go unnoticed. I also want to thank you for being there to discuss teaching methods and problems with me. I hope we can continue to have discussions about such things in the future. Finally, I thank Jim, without whom I would not be here today. Thank you for your guidance. Thank you for taking the time to develop my writing skills. Thank you (and Susan) for welcoming me into your home and your life. Thank you for introducing me to the wonder that is Kilauea. I will, one day, fulfill my promise to write some incredible papers on the intimate relationship between tectonic and volcanic processes at Kilauea. And most of all, thank you for your patience. I know I have been difficult at times, often persistent, not to mention a real pain in the ass. But you have been amazing. I look forward to collaborating with you in the future.

None of this would have been possible without Keith Richards-Dinger. Your programming skills are unmatchable. Thank you for always being available to answer my questions, especially the stupid ones, and for being able to quickly identify when I am missing a parentheses or a comma. One day I will learn.

Thank you, Robert Valdez, for taking on the tedious project of measuring countless angles and speeds of propagation. Without our help (and focus) it would have taken me another year to finish my dissertation.

I would also like to thank Kayla Kroll and Steven Bates for proof reading and editing “final” versions of manuscripts. If it were not for them manuscripts would have been submitted with additional errors and nonsensical sentences.

I would be amiss if I did not thank Dave Bowman. You have been my advisor, mentor, and friend. I feel so fortunate to have found you along this journey. As an undergraduate, you introduced me to research. You took the time to have long discussions with me about graduate school, which led me to Jim and, subsequently. a project that I love. As a graduate student, you have always been there to give me advice about options for the future. Additionally, thank you for always make time for me at conferences, particularly early on when I did not know anyone. I always look forward to our nights out. I hope to continue to have a sushi and cigars (or hookah) night or dueling piano night with you at every conference. And one day I will finish a “Car Bomb” faster than you!

To Steve – No matter where we are or what becomes of us you will forever be a piece of me. Your love and support throughout this journey has meant the world to me. We both know it has not been easy to do either one. I appreciate all you have done for me.

None of this would be possible without the love and support from my family. To my mom – I know sometimes you think you may have created a monster with how independent I am, but without the ability to carve my own path, which you instilled in me at a young age, I would not be here. I cannot thank you enough (although I am sure Steve hates you for that). To my daddy – Thank you for always believing in me even when you didn't want to (e.g. like when I quit school). Thank you for all the love you give me every day. Sister – you are one of my closest friends. You tell it to me straight and are always there when I need you. And last, don't worry I am not leaving you out, my baby brother. It means more to me than I can ever express that you come to me with questions about geology (e.g. oil companies to invest in and why there is a big meteor crater in northern Arizona). I am so proud of the man you have become. As dysfunctional as we all are, I feel very lucky to be part of this family. Today would not be have happened without your love and encouragement over the last 5 ½ years. I love you all so much.

Finally, the text of this dissertation, in part, is a slightly edited version of a paper published by AGU (Chapter 2 - Methods and Chapter 3). Copyright (2011) American Geophysical Union. The full citation of the paper is "Colella, H. V., J. H. Dieterich, K. Distance along dip (km)B. Richards-Dinger, (2011), Multi-event simulations of slow slip events for a Cascadia-like subudction zone, Geophysical Research Letters, *38*, L16312, doi:10.10229/2011GL0488141. The co-author, James Dieterich, listed in the publications directed and supervised the research, which forms the basis from this dissertation. Keith Richards-Dinger developed and maintained the code used for simulations.

Dedication

To my baby love

You changed me. My life is not the same without you.

ABSTRACT OF THE DISSERTATION

Complex Characteristics of Slow Slip Events and Their Influence on Subduction Zone Dynamics Based on Multi-Cycle Simulations

by

Harmony Colella

Doctor of Philosophy, Graduate Program in Geological Sciences
University of California Riverside, December 2011
Dr. James H. Dieterich, Chairperson

The recent discovery of slow slip events (SSEs) in subduction zones has resulted in a variety of new observations that are modeled using the new, physics-based, computationally efficient, earthquake simulation code, RSQSim. RSQSim fully incorporates 3D elastic stress interactions and employs rate- and-state constitutive properties for the sliding strength of faults. RSQSim is capable of generating 100,000s of slip events, which is ideal to understand the long-term characteristics of SSEs and their interactions with adjacent sections of the megathrust. For the simulations presented here, I adopt a Cascadia-like model of the subduction zone interface, where the megathrust is divided into three sections with different sliding characteristics: locked, transition, and continuous creep. The locked zone (<25 km depth) corresponds to the section of the megathrust that generates great earthquakes, the transition zone (~25-45 km depth)

corresponds to the section of the megathrust that generates SSEs, and the continuous creep zone (>45 km depth) corresponds to the section at depth that slides continuously. Results from the simulations are in broad agreement with the characteristics of observed SSEs, for example, their average durations, inter-event times, and slip. The simulations produce complex, high-resolution slip patterns that are remarkably similar to tremor migration patterns observed during SSEs in Cascadia and Nankai. Additionally, the results show a depth-dependence of the characteristics of slip in the transition zone, where the frequency of slip increases with increasing depth. The depth-dependence of slip, and subsequently stress, suggests a spectrum of behaviors along a subduction zone interface, is, in part, related to the creeping zone adjacent to, and below, the transition zone and, in part, related to the constitutive properties in the transition zone. The stressing rate on the seismogenic zone is ~100x higher during a SSE than during the inter-SSE period, which may give rise to increased activity in the highly stressed region or may initiate nucleation of a great earthquake. Finally, the simulations show a significant slip deficit in the transition zone, which may have significant implications for seismic hazards for coastal cities near subduction zones.

Table of Contents

List of Figures

List of Tables

List of Equations

Chapter 1

Introduction

Subduction zones generate the world's largest earthquakes ($M_w \geq 8$). These great earthquakes release 100s of years of accumulated strain in just a few minutes, which results in intense ground shaking over large regions. The displacement of the sea floor in in these events generates tsunamis like those of the great 2004 Sumatra and 2011 Japan earthquakes. It has been recently discovered that subduction zone megathrusts also periodically release stored elastic strain energy through 'slow slip events' (SSEs). SSEs involve slow slip (~10 km/day) on the subduction zone interface, which is much slower than traditional earthquake slip (~2-3 km/sec). SSEs have durations of weeks to months and are accompanied by non-volcanic, or tectonic, tremor. While SSEs appear to be a harmless relative to their earthquake cousins, the largest SSEs may occur up to several times per year and involve sustained fault slip directly down-dip of the base of the seismogenic section in subduction zones – i.e. the source region of megathrust earthquakes. Repeated SSEs may load the up-dip seismogenic section, bringing it closer to failure. Thus improved understanding of SSEs and their interactions with megathrust earthquakes are important for seismic hazard assessment.

1.1 Sliding mechanisms in subduction zones

Great earthquakes occur as a result of the release of 10s-1000s of years of strain energy accumulated along the "locked" section of the subduction zone as an oceanic plate tries to subduct beneath an overriding plate (Figure 1). Friction on the interface causes the plates to remain locked, while the surrounding lithosphere bends under the forces of subduction, which results in accumulation of elastic stress and strain. When the elastic stress is large enough to overcome friction, it is released in rapid, unstable fault slip under rate-weakening conditions, wherein the fault weakens as friction decreases with increasing slip speed. With increasing depth, and thus increasing temperature, rate-weakening behavior diminishes and gives way to rate-strengthening, whereby the fault strengthens as friction increases with increasing slip speed, which inhibits earthquakes and results in stable sliding. Theory predicts a transition zone between unstable and stable sliding [*Tse and Rice,* 1986], but until recently there have been few observations that illuminate the fault behavior in the transition zone.

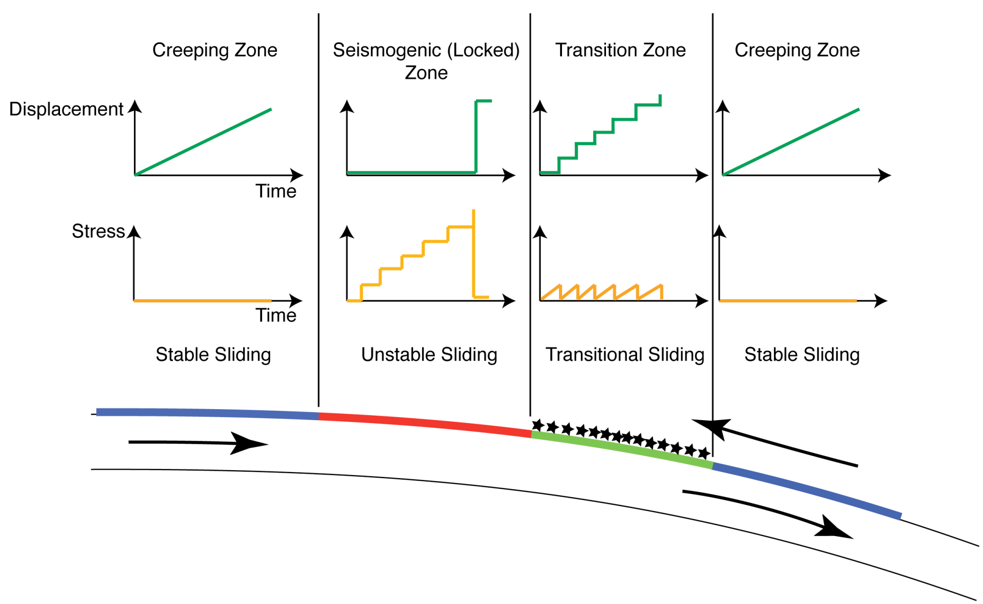

Figure 1.1: *Conceptual model of a subduction zone illustrating plate motion and stress accumulation across the plate interface. Relative displacements and shear stress changes are sketched as a function time. Stars represent the suspected source region of tremors associated with slow slip events. [modified from Dragert et al., 2004].*

Sliding behaviors analogous to those observed in subduction zones are also produced in laboratory fault-slip experiments [*Blanpied et al.,* 1998; *He et al.*, 2007], where sliding processes and constitutive parameters can be studied directly. The observed frictional dependencies have been successfully modeled with rate- and state-dependent formulations. *Ruina* [1983] simplified the *Dieterich* [1979; 1981] formulation for resistance to slip to be written as:

$$\tau = \sigma\left[\mu_0 + a\ln\left(\frac{\dot{\delta}}{\dot{\delta}^*}\right) + b\ln\left(\frac{\theta}{\theta^*}\right)\right] \tag{1.1}$$

where μ_0 , *a*, and *b* are experimentally determined constants; $\dot{\delta}$ is sliding speed, θ is a state variable that evolves with time, slip, and normal stress history; and $\dot{\delta}^*$ and θ^* are normalizing constants. A necessary condition for unstable earthquake slip, or rate-weakening, is $(b - a) > 0$ at steady-state. Conversely, if $(b - a) < 0$ the fault slip is continuous, stable creep, or rate strengthening. Transitional behavior is expected when $(b - a) \approx 0$.

1.2 History of research into slow slip events

New opportunities to investigate fault-slip behavior emerged when *Dragert et al.*, [2001] detected a slow release of strain accumulation equivalent in size to a M_w6.7 earthquake in the Vancouver Island-Puget Sound region of the Cascadia subduction zone in continuous GPS data. Unusually, the strain release was not accompanied by a large earthquake. This event lasted ~2 weeks, during which the locus of deformation migrated northwestward several hundred kilometers, and was inferred to represent ~2 cm of accelerated thrust slip on the subduction zone interface between depths of 25 to 45 km, in the theoretically predicted transition zone [*Dragert et al.*, 2001] (Figure 2). This event was referred to as a 'silent slip event' because, initially, it was not associated with a seismic signal. These events were renamed 'episodic tremor and slip', when *Dragert et al.* [2004] identified additional silent slip events in northern Cascadia all of which were associated with tectonic tremor. Similar events have since been observed in several

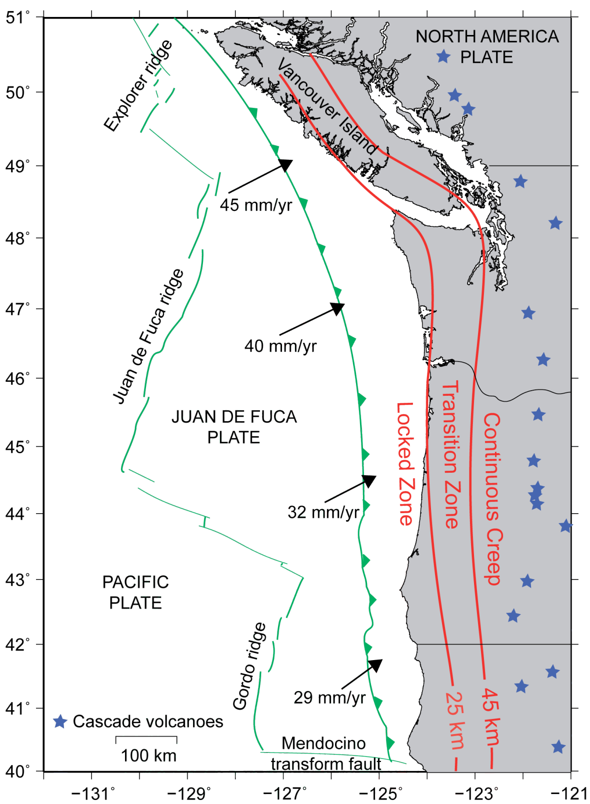

Figure 1.2: *Map of Cascadia Subduction Zone, where red contours indicate depth of interface [modified from McCroy et al., 2004].*

subduction zones (*Hirose et al.*, 1999; *Lowry et al.*, 2001; *Obara*, 2002; *Kostoglodov et al.*, 2003; *Protti et al.,* 2004; *Douglas et al.*, 2005, *Ohta et al.*, 2006], transform plate boundaries [*Linde et al.*, 1996], and the decollement underlying Kilauea volcano, Hawai'i [*Cervelli et al.*, 2002; *Brooks et al.*, 2006]. It is important to note that in some cases only one of the two phenomena is observed. The slip portion is now most commonly referred to as a ‘slow slip event’, or SSE.

In subduction zones with dense seismic and geodetic networks, tectonic tremor is often observed coincident with SSEs (Figure 1). Tectonic tremor is characterized as a long-duration, low amplitude, continuous seismic signal without distinct P or S arrivals with durations of hours to weeks, and periods of increasing and decreasing amplitudes. The Japan Meteorological Agency (JMA) was the first to identify low-frequency earthquakes (LFEs) within the tectonic tremor of the Shikoku subduction zone. *Shelly et al.* [2007a] isolated pulse-like signals between 1 and 10 Hz with equivalent moment magnitude of ~M_w1.0 and noted that the seismic spectra of LFEs is quite similar to that of tectonic tremor. They deduced that tectonic tremor was the superposition of numerous, continually occurring LFEs. LFEs in Cascadia and Nankai subduction zones exhibit similar spatiotemporal relationships as SSEs [*Dragert et al.*, 2004; *Obara and Hirose*, 2006; *Aguiar et al.*, 2009]. *Ito et al*. [2007] detected anomalous very low-frequency earthquakes (VLFEs) between 0.02-0.05 Hz with equivalent moment magnitude of ~M_w3.2-3.8 within tremor bursts in the regions of Tokai, northeastern Kii, and western Shikoku, Japan. VLFEs have also been detected near the updip edge of the seismogenic zone, adjacent to the shallow creeping zone, near the accretionary wedge [*Obara,* 2011]. Focal mechanism solutions for VLFEs indicate the events occur as shear slip on a shallow thrust faults in the direction of subduction, which suggests slow slip and tremor share a common underlying physical process [*Ide et al*., 2007]. Because tectonic tremor is observed coincident with SSEs in Cascadia and Japan where the subduction zones are well-instrumented, tremor is often used as a proxy for slow slip where global positioning system (GPS) data is unavailable or detection limits are not met [*e.g. Peng and Gomberg*, 2010].

High-resolution tremor observations in Cascadia and Nankai indicate highly complex spatiotemporal migration patterns during individual SSEs. Some complexities include slow, incoherent initiation and termination of events [*Houston et al.*, 2011], simultaneous slip in multiple locations [*Boyarko and Brudzinski*, 2010; *Obara*, 2010], rapid tremor reversal [*Houston et al.*, 2011] and along-dip tremor streaks [*Shelly et al.*, 2007b; *Ghosh et al.*, 2010; 2011].

SSEs can be separated into two classes based on their duration and periodicity: long-term SSEs and short-term SSEs. Long-term SSEs last years with recurrence intervals 4-10 years. Such events have been identified in Nankai in the Bungo Channel [*Hirose and Obara*, 2005] and Tokai region of Japan [*Suito and Ozawa*], Hikaurangi, New Zealand [*Wallace and Beavan*, 2010], Guerrero, Mexico [*Vergnolle et al.*, 2010], and Alaska [*Peterson and Christensen*, 2009]. Short-term SSEs last days to weeks with recurrence intervals of days to months. Such events have been identified in Cascadia [*Brudzinski and Allen*, 2007; *Aguiar et al.*, 2009; *Schmidt and Gao*, 2010], Hawai'i [*Cervelli et al.*, 2002; *Brooks et al.*, 2006] and Nankai in the Shikoku and Kii regions [*Obara*, 2010; *Sekine et al.*, 2010]. The variation in durations and recurrence intervals in the same region (along the same subduction zone) suggests segmentation of the megathrust.

SSEs in subduction zones are typically observed between 25 km and 45 km depth, between the seismogenic zone up-dip and the continuous creep zone down-dip [*Dragert et al.,* 2001; 2004; *Obara et al.*, 2004]. However, SSEs have been detected at shallow depths (~5 km) between the seismogenic zone and continuous creep zone (Figure 1) [*Hirose and Obara*, 2005; *Wallace and Beavan*, 2010]. In Hawai'i, SSEs occur ~8 km between the seismogenic section of Kilauea's decollement and the rift zone [*Cervelli et al.*, 2002]. Shallow SSEs have also been identified in the creeping section of the San Andreas [*Langbein et al.*, 1990; *Linde et al.*, 1996], Hayward [*Lienkaemper et al.*, 1997], Superstition Hills [*Wei et al.*, 2009], and Calaveras [*McFarland et al.*, 2009] faults. While the duration and recurrence time of SSEs vary dramatically from one region to the next, it appears that they consistently occur in regions between the seismogenic and creeping sections of a fault where there is a transition in frictional behavior.

1.3 Remaining questions

SSEs have been observed in subduction zones, transform plate boundaries, and, recently, at Kilauea volcano. SSEs likely result from a transition in frictional behavior in the regime between unstable and stable sliding, however the physical mechanism that produces slow slip is still unknown. The occurrence of tectonic tremor with SSEs in subduction zones, and the absence of high-frequency energy in that tremor, has led some to suggest pore fluid pressures produced by dehydration of the oceanic slab play a key role in slow slip [*Obara*, 2002; *Dragert et al.*, 2004; *Ito et al.*, 2007], where high pore fluid pressures reduce the effective normal stress along the plate interface. In addition, the observed variation in durations, recurrence intervals and locations of SSEs worldwide, and within individual subduction zones, suggests fundamentally different structural and/or mechanical properties may also affect the occurrence of SSEs.

The correlation of tectonic tremor with SSEs, particularly in subduction zones, raises questions with regards to the process, or processes, that cause tremor to occur, the relationship between tremor and slow slip, and what causes tremor migration patterns to be so complex. *Ito et al.* [2007] presents one possible scenario: the asperity model, in which strongly coupled patches are surrounded by aseismic, slow slip regions. In this scenario, the fault shears at very low shear strength because of the presence of fluids. LFEs and VLFEs are generated by patches with stronger rate-weakening properties, while the rest of the fault moves aseismically. As for complex tremor patterns, various processes have been proposed that may influence these complex patterns, however neither a physical mechanism nor a quantitative model has been agreed upon [*Ando et al.*, 2009; Houston *et al.,* 2010; *Ghosh et al.,* 2010; 2011; *Ide*, 2010; *Rubin*, 2011].

Identification of SSEs in subduction zones has also raised concerns with regards to their relationship to great earthquakes, specifically their impact on seismic hazards for coastal communities. Coulomb stress calculations for ETS events suggest that they cause a temporary stressing rate increase up-dip on the adjacent seismogenic zone, which could potentially trigger a great, megathrust earthquake [*Dragert et al.*, 2004]. Additionally, it had been assumed that a great earthquake would only rupture to ~25 km depth, which is approximately the coastline of western North America (Figure 1). If, however, the transition zone in which SSEs occur slipped seismically, the rupture zone could be much larger. For example, *Burgette et al.* [2009] and *Chapman and Melbourne* [2009] suggest the down-dip edge of the seismogenic zone in Cascadia could extend ~30 and ~60 km farther inland than previously determined in southern Oregon and Washington, respectively.

This study simulates SSEs along a subduction zone interface to explore their unusual characteristics and their effects on the adjacent sections of the megathrust. I employ the earthquake simulation code, RSQSim (described in Chapter 2), which generates long histories of SSEs to 1) better understand the interactions of multiple sliding mechanisms along a fault, 2) investigate the characteristics and complexities of SSEs, and 3) explore the relationship between SSEs and great, megathrust earthquakes. Chapter 2 provides details of the modeling technique employed for this study. In Chapter 3, I use a simple, idealized configuration of a Cascadia-like subduction zone with multiple sliding mechanisms to explore the characteristics of SSEs. This is the first study of its kind to simulate long histories of SSEs. It provides the opportunity to explore their characteristics over 100s of cycles and their interactions with the adjacent sections of the megathrust. It also serves as a validation of the modeling technique. In Chapter 4, the fault model is modified to include a larger transition zone with a gradient in frictional properties to investigate the complex migration patterns of SSEs/ETS events. The results agree remarkably well with observed tremor migration patterns and thus provide a potential explanation for some of the complexities observed in SSEs. Finally, Chapter 5 explores the depth-dependent characteristics of slip within the transition zone. Results from these simulations support the conceptual model of subduction zone dynamics presented by *Wech and Creager* [2011], wherein convergence is accommodated through a continuum of slip, stress, and strength behaviors. This simulations also suggest a slip deficit within the transition zone, which may affect the down-dip rupture extent of great earthquakes along subduction zone and, consequently, have significant implications for hazard assessments near subduction zone margins.

1.4 References

Aguiar, A. C., T. I. Melbourne, and C. W. Scrivner (2009), Moment release of Cascadia tremor constrained by GPS, *J. Geophys. Res.*, *114*, B00A05, doi:10.1029/2008JB005909.

Blanpied, M. L., D. A. Lockner, and J. D. Byerlee (1991), Fault stability inferred from granite sliding experiments at hydrothermal conditions, *Geophys. Res. Lett.*, *18*, 609-612, doi:10.1029/91GL00469.

Blanpied, M. L., C. J. Marone, D. A. Lockner, J. D. Byerlee, and D. P. King (1998), Quantitative measure of the variation in fault rheology due to fluid-rock interactions, *J. Geophys. Res., 103*(B5), 9691 – 9712, doi:10.1029/98JB00162.

Boyarko, D. C. and M. R. Brudzinski (2010), Spatial and temporal patterns of nonvolcanic tremor along the southern Cascadia subduction zone, *J. Geophys. Res., 115*, B00A22, doi:10.1029/2008JB006064.

Brooks, B. A., J. H. Foster, M. Bevis, L. N. Fazer, C. J. Wolfe, and M. Behn (2006), Periodic slow earthquakes on the flank of Kilauea volcano, Hawai'i, *Earth Planet. Sci. Lett.*, *246*, 205-216.

Brudzinski, M. R., and R. Allen (2007), Segmentation in episodic tremor ad slip all along Cascadia, *Geology, 35*(10), 907-910, doi:10.1130/G23740A.1.

Burgette, R. J., R. J. Weldon II, and D. A. Schmidt (2009), Interseismic uplift rates from western Oregon and along –strike variations in locking on the Cascadia subduction zone, J. Geophys. Res., 114, B01408, doi: 10.1029/2008JB005679.

Cervelli, P., P. Segall, K. Johnson, M. Lisowski, and A. Miklius (2002), Sudden aseismic fault slip on the south flank of Kilauea volcano, *Nature*, *415*, 1014-1018.

Chapman, J. S., and T. I. Melbourne (2009), Future Cascadia megathrust rupture delineated by episodic tremor and slip, Geopyhys. Res. Lett., 36, L22301, doi: 10.1029/2009GL040465.

Colella, H. V., J. H. Dieterich, K. B. Richards-Dinger (2011), Multi-event simulations of slow slip events for a Cascadia-like subduction zone, *Geophys. Res. Lett., 38*, L16312, doi:10.1029/2011GL048817.

Dieterich, J. H. (1979), Modeling of rock friction 1. Experimental results and constitutive equations, *J. Geophys. Res., 84*(B5), 2161 – 2168, doi:10.1029/JB084iB05p02161.

Dieterich, J. H. (1981), Constitutive properities of faults with simulated gouge, in Monograph 24, Mechanical behavior of crustal rocks, edited by N. L. Carter, M. Friedman, J. M. Logan, and D. W. Sterns, Am. Geophys. Union, Washington, D. C., 103-120.

Douglas, A., J. Beavan, L. Wallace, J. Townend (2005), Slow slip on the northern Hikurangi subduction interface, New Zealand, *Geophys. Res. Lett., 32*, L16305, doi: 10.1029/2005GL023607.

Dragert, H., K. Wang, and T. S. James (2001), A silent slip event on the deeper Cascadia subduction interface, *Science, 292*, 1525–1528, doi:10.1126/science.1060152.

Dragert, H., K. Wang, and G. Rogers (2004), Geodetic and seismic signatures of episodic tremor and slip in the northern Cascadia subduction zone, *Earth Planets Space, 56*(12), 1143–1150.

He, C., Z. Wang, and W. Yao (2007), Frictional sliding of gabbro gouge under hydrothermal conditions, *Tectonophysics*, 445, 353 – 362, doi:10.1016/j.tecto. 2007.09.008.

Hirose, H., and K. Obara (2005), Repeating short- and long-term slow slip events with deep tremor activity around the Bungo channel region, southwest Japan, *Earth Planets Space, 57*, 961-972.

Hirose, H., K. Hirahara, F. Kimata, N. Fujii, and S. Miyazaki (1999), A slow thrust slip event following the two 1996 Hyuganada earthquakes beneath the Bungo Channel, southwest Japan, *Geophys. Res. Lett., 26*, 3237–3240, doi:10.1029/1999GL010999.

Ghosh, A., J. E. Vidale, J. R. Sweet, K. C. Creager, A. G. Wech, H. Houston, and E. E. Brodsky (2010), Rapid, continuous streaking of tremor in Cascadia, *Geochem. Geophys. Geosyst.*, *11*, Q12010, doi:10.1029/2010GC003305.

Ghosh, A., J. E. Vidale, and K. C. Creager (2011), paper presented at the Annual Seismological Society of America, Memphis, TN, 13-15 April.

Houston, H., B. G. Delbridge, A. G. Wech, and K. C. Creager (2011), Rapid tremor reversals in Cascadia generated by a weakened plate interface, *Nature Geosci.*, *4*, 404-409, doi:10.1038/ngeo1157.

Ide, S. (2010), Striations, duration, migration and tidal response in deep tremor, *Nature*, *466,* 356-359, doi:10.1028/nature09251.

Ide, S., D. R. Shelly, and G. C. Beroza (2007), Mechanism of deep low frequency earthquakes: Further evidence that deep non-volcanic tremor is generated by shear slip on the plate interface, Geophys. Res. Lett., 34, L03308, doi:10.1029/2006GL028890.

Ito, Y., K. Obara, K. Shiomi, S. Sekine, and H. Hirose (2007), Slow earthquakes coincident with episodic tremors and slow slip events, *Science, 315*, 503-506.

Kodaira, S., T. Iidaka, A. Kato, J. O. Park, T. Iwasaki, and Y. Kaneda (2004), High pore fl uid pressure may cause silent slip in the Nankai Trough: Science, *304*, p. 1295–1298, doi: 10.1126/science.1096535.

Langbein, J., R. Burford, and L. Slater (1990), Variations in fault slip and strain accumulation at Parkfield, California: Initial results using two-color geodimeter measurements, 1984–1988, *J. Geophys. Res.*, *95*, 2533– 2552.

Lienkaemper, J. J., J. S. Galehouse, and R. W. Simpson (1997), Creep response of the Hayward Fault to stress changes caused by the Loma Prieta earthquake, *Science, 276*, 2014-2016, doi:10.1126/science.276.5321.2014.

Lowry, A. R., K. M. Larson, V. Kostoglodov, and R. Bilham (2001), Transient fault slip in Guerrero, southern Mexico, *Geophys. Res. Lett., 28*, 3753– 3756, doi: 10.1029/2001GL013238.

McCrory, P. A., J. L. Blair, D. H. Oppenheimer, and S. R. Walter (2004), Depth to the Juan de Fuca slab beneath the Cascadia subduction margin: A 3-D model for sorting earthquakes, *U.S.G.S. Data Series DS-91*, 1 CD-ROM, version 1.2.

McFarland, F., J. Lienkaemper, and S. J. Caskey, Data from theodolite measurements of creep rates on San Francisco Bay region faults, California; 1979-2009, *USGS Open file report 09-1119*, 2009.

Miller, M. M., T. Melbourne, D. J. Johnson, W. Q. Sumner (2002), Periodic slow earthquakes from the Cascadia subduction zone, *Science*, *295*, 2423.

Obara, K. (2002), Nonvolcanic deep tremor associated with subduction in southwest Japan, *Science, 296*, 1679 – 1681, doi:10.1126/science.1070378.

Obara, K. (2010), Phenomenology of deep slow earthquake family in southwest Japan: spatiotemporal characteristics and segmentation, *J. Geophys. Res., 115*, B00A25, doi: 10.1029/2008JB006048.

Obara, K. (2011), Characteristics and interactions between non-volcanic tremor and related slow earthquakes in the Nankai subduction zone, southwest Japan, *J. Geodynamics, 52*, 229-248.

Obara, K., and H. Hirose (2006), Non-volcanic deep low-frequency tremors accompanying slow slip in the southwest Japan subduction zone. *Technophysics, 417*, 33-51.

Ohta, Y., Freymueller, J. T., Hreinsdottir, S., and Suito, H. (2006), A large slow slip event and the depth of the seismogenic zone in the south central Alaska subduction zone, *Earth Planet. Sci. Lett., 247*, 108-116, doi:10.1016/epsl.2006.05.013.

Peng, Z., and J. Gomberg (2010), An integrated perspective of the continuum between earthquakes and slow-slip phenomena, *Nature Geosci., 3*, doi:10.1038/NGEO0940.

Peterson, C., and D. Christensen (2009), Possible relationship between non-volcanic tremor and the 1998-2001 slow-slip event, south central Alaska*, J. Geophys. Res., 114*, B06302, doi:10.1029/2008JB006096.

Protti, M., V. Gonzales, T. Kato, T. Iinuma, S. Miyasaki, K. Obana, Y. Kaneda, P. LaFemina, T. Dixon, and S. Schwartz (2004), A creep event on the shallow interface of the Nicoya Peninsula, Costa Rica seismogenic zone, *Eos Trans. AGU, 85*(47), Fall Meet. Suppl., Abstract S441D-07.

Rice, J. R. (1983), Constitutive relations from fault slip and earthquake instabilities*, Pure Appl. Geophys., 121*, 443-475, doi:10.1007/BF02590151.

Rogers, G., and H. Dragert (2003), Episodic tremor and slip on the Cascadia subduction zone: The chatter of silent slip, *Science, 300*, 1942 – 1943, doi:10.1126/science.1084783.

Schmidt, D. A. and H. Gao (2010), Source parameters and time-dependent slip distribution of slow slip events on the Cascadia subduction zone from 1998 to 2008, *J. Geophys. Res., 115*, B00A18, doi:10.1029/2008JB006045.

Schwartz, S. Y., and J. M. Rokosky (2007), Slow slip events and seismic tremor at circum-Pacific subduction zones, *Rev. Geophys., 45*, RG3004, doi: 10.1029/2006RG000208.

Segall, P., A. M. Rubin, A. M. Bradley, and J. R. Rice (2010), Dilatant strengthening as a mechanism for slow slip events, *J. Geophys. Res., 115*, B12305, doi: 10.1029/2010JB007499.

Sekine, S., H. Hirose, and K. Obara (2010), Short-term slow slip events correlated with non-volcanic tremor episodes in southwest Japan, *J. Geophys. Res., 115,* doi: 10.1029/2008JB006059.

Shelly, D. R., G. C. Beroza, S. Ide, and S. Nakamula (2006), Low frequency earthquakes in Shikoku, Japan, and their relationship to episodic tremor and slip, *Nature, 442*, 188–191, doi:10.1038/nature04931.

Shelly, D. R., G. C. Beroza, and S. Ide (2007a), Non-volcanic tremor and low-frequency earthquake swarms, *Nature, 446*, 305–307, doi:10.1038/ nature05666.

Shelly, D. R., G. C. Beroza, and S. Ide (2007b), Complex evolution of transient slip derived from precise tremor locations in western Shikoku, Japan, *Geochem. Geophys. Geosyst., 8*, Q10014, doi:10.1029/2007GC001640.

Suito, H., and T. Ozawa (2009), Transient crustal deformation in the Tokai district, *J. Seismol. Soc. Jpn., 2*(61), 113-115.

Vergnolle, M., A. Walpersdorf, V. Kostoglodov, P. Tregoning, J. A. Santiago, N. Cotte, and S. I. Franco (2010), Slow slip events in Mexico revised from the processing of 11 year GPS observations, *J. Geophys. Res., 115*, B08403, doi:10.1029/2009JB006852.

Wallace, L. M., and J. Beavan (2010), Diverse slow slip behavior at the Hikurangi subduction margin, New Zealand, *J. Geophys. Res., 115*, B12402, doi: 10.1029/2010JB007717.

Wech, A. G., and K. C. Creager (2011), A continuum of stress, strength and slip in the Cascadia subduction zone, *Nature Geosci.*, doi:10.1038/NGEO01215.

Wei, M., D. Sandwell, and Y. Fialko (2009), A silent Mw 4.7 slip event of October 2006 on the Superstition Hills fault, southern California, *J. Geophys. Res.,* 114, B07402.

Chapter 2

Methods

Portions originally published in *Geophysical Research Letters* as supplementary material and in review with *Science* as supplementary material

Colella, H. V., J. H. Dieterich, K. B. Richards-Dinger (2011), Multi-event simulations of slow slip events for a Cascadia-like subudction zone, *Geophys. Res. Lett.*, *38*, L16312, doi:10.10229/2011GL0488141.

2.1 Previous approaches

Previous modeling studies of slow slip events (SSEs) employ rate- and state-dependent constitutive laws, and largely focus on possible mechanisms that quench the acceleration of slip during the nucleation process of SSEs before earthquake slip speeds are reached. *Shibazaki and Iio* [2003] employed a variant of rate-state friction that causes steady state friction to oscillate between rate-weakening at low slip speeds and rate-strengthening at high slip speeds, which serves to quench runaway acceleration of slip speed that would otherwise produce earthquake slip. *Liu and Rice* [2005; 2007] and *Rubin* [2008] show that SSEs can arise under conditions near the boundary between stable and unstable slip, namely small positive values of (b - a) in combination with low effective normal stress. Small positive values of (b - a) may be expected in the transition zone between the seismogenic and creeping sections; and low effective normal stresses from dehydration reactions are indicated by thermal modeling [*Peacock et al.*, 2002] and seismological observations [*Kodaira et al., 2004*; *Shelly et al.*, 2006].

2.2 RSQSim

For the work presented here, I employ the fault slip and earthquake simulation code Rate-State Quake Simulator, or RSQSim. The code was developed to generate synthetic statistical distributions of earthquakes (synthetic catalogs) for probabilistic estimation, with particular interest in California [*Dieterich and Richards-Dinger*, 2010]. Here, I use RSQSim to generate synthetic catalogs of SSEs. The very short observation period of SSEs (~10-15 years) makes RSQSim an ideal tool to explore these events over

100s of cycles. Additionally RSQSim may shed light on the relationship between SSEs and great earthquakes.

To develop robust statistical characterizations of SSEs, and to investigate how SSEs interact with the adjacent sections of the mega-thrust interface, the simulations incorporate the three slip modes observed in a subduction zone: earthquake slip, slow slip, and continuous creep. Long histories of slip events (10^6 - 10^7 earthquakes and/or SSEs) are generated to evaluate potential earthquake probabilities associated with SSEs. Repeated simulations will be used to explore the sensitivity of the results to model parameters.

RSQSim uses 3D boundary elements based on dislocation solutions for rectangular fault elements [*Okada*, 1992]. It is capable of modeling earthquake slip, slow slip events, and continuous fault creep. It accepts different modes of faulting (normal, reverse, strike-slip) as well as mixed slip modes. Interactions among the fault elements are represented by an array of 3D elastic dislocations, where stresses acting on the centers of the elements are:

$$\tau_i = K_{ij}^{\tau}\delta_i + \tau_i^{tect} \quad (2.1)$$

$$\sigma_i = K_{ij}^{\sigma}\delta_i + \sigma_i^{tect} \quad (2.2)$$

where *i* and *j* run from 1 to *N*, the total number of fault elements; τ_i and σ_i are the shear stress in the prescribed rake direction and fault-normal stress on the i^{th} element, respectively; K_{ij}^{τ} and K_{ij}^{σ} are interaction matrices derived from elastic dislocation solutions; δ_i is slip of fault element *j*; τ_i^{tect} and σ_i^{tect} represent stresses applied to the i^{th}

element by sources external to the fault system (such as far field tectonic motions); and the summation convention applies to repeated indices.

The model employs a rate- and state-dependent formulation for resistance to slip across each fault element [*Dieterich* 1979; 1981; *Rice,* 1983; *Ruina*, 1983]:

$$\tau = \sigma\left[\mu_0 + a\ln\left(\frac{\dot{\delta}}{\dot{\delta}^*}\right) + b\ln\left(\frac{\theta\dot{\delta}^*}{D_c}\right)\right], \tag{2.3}$$

where τ and σ are the shear and normal stress, respectively, acting on a fault element during slip, μ_0 is the nominal coefficient of friction, a and b are experimentally determined constants with values that generally range from 0.008-0.015; $\dot{\delta}$ is slip speed; θ is a state variable that evolves with time, normal stress, and over a characteristic slip distance D_c, 10^{-5} m in these simulations; and $\dot{\delta}^*$ is a normalizing constant.

These simulations employ the aging form of the state evolution law with the effects of changes in normal stress from [*Linker and Dieterich*, 1992]*:*

$$\dot{\theta} = 1 - \frac{\dot{\delta}\theta}{D_c} - \frac{\alpha\theta\dot{\sigma}}{b\sigma}, \tag{2.4}$$

where α =0.25 in these simulations. At constant normal stress, the evolution of θ takes place over a characteristic distance D_c and, for a constant slip speed $\dot{\delta}$, will approach a steady-state of $\theta_{ss} = D_c/\dot{\delta}$.

A central feature of RSQSim is the use of event-driven computational steps for modeling slip events (earthquakes and SSEs) as opposed to time stepping at closely spaced intervals [*Dieterich*, 1995]. The cycle of stress accumulation and slip at each fault element is separated into three distinct phases designated as sliding states 0, 1, and 2. For each of these states, there are approximate analytic expressions for the evolution of stress, slip, slip speed, and state variable. A fault element is at state 0 when stress is below the steady-state friction, as defined by rate- and state-dependent friction. In the model this condition is approximated as a fully locked element, where the fault strengthens as the frictional state-variable θ increases with time, *e.g.,* $\theta = \theta_0 + t$ at constant normal stress, but modified by effects arising from normal stress changes using equation (Eq. 2.4).

The transition to sliding state 1, or nucleation, occurs when the stress exceeds steady-state friction. During state 1, conditions have not yet been met for rupture propagation, but the state progressively decreases as described by rate- and state-dependent fault constitutive properties, leading ultimately to acceleration to SSE or seismic slip speeds. For both earthquakes and SSEs the analytic solutions for nucleation [*Dieterich*, 1992*; Fang et al.*, 2010], together with stressing rates, determine the transition time to state 2 (SSE or seismic slip). At tectonic stressing rates, event nucleation may require days to years, depending on constitutive parameters and normal stress, but during propagation of SSE or seismic ruptures the high stress rates at the rupture front compress the duration of state 1 to a few hours or a fraction of a second, respectively. Hence, during rupture propagation, state 1 in effect forms a process zone at the rupture front where time-dependent breakdown of fault strength occurs. The slip during nucleation is negligible compared to slip during rupture and is therefore ignored for purposes of computing stress changes on other elements.

During states 0 and 1, RSQSim uses the quasi-static approximation: the applied shear stress on each fault element (Eq. 2.1) is balanced by the frictional shear stress (Eq. 2.3). In the case of seismic slip, this approximation breaks down as the slip accelerates in state 1, and inertial effects act to quench the maximum slip speed. In this (seismic) case, the model employs a quasi-dynamical representation of the gross dynamics of the earthquake source based on the relationship for elastic shear impedance together with the local dynamic driving stress. From the shear impedance relation [*Brune*, 1970] the fault slip rate is:

$$\dot{\delta}^{EQ} = \frac{2\beta\Delta\tau}{G} \tag{2.5}$$

where the driving stress $\Delta\tau$ is the difference between the stress at the initiation of slip and the sliding friction; β is the shear wave speed; and G is the shear modulus. An element transitions from state 1 to state 2 when its slip speed accelerates to that given by the above shear impedance relation, and its slip speed is held at this value until the patch reverts to state 0. This provides a first-order representation of dynamical time-scales and slip rates for the coseismic portion of the earthquake simulations. An element ceases to slip and transitions back to state 0 when the stress decreases to some specified stress determined by the steady-state friction at the seismic slip speed (with inertial overshoot of stress to levels less than this friction level as an adjustable model parameter, which is discussed below). In the case of SSEs the mechanism that quenches the slip speeds at values far below seismic slip speeds is still unclear. In this study, SSEs are modeled the same way as earthquakes except slip speed is set to a much lower value (~10^{-6} m/s) based on observations of SSE slip and event durations.

Determination of the sliding state changes requires computation of the stress state as a function of time at each fault element. Note that stressing rates are constant between state changes and the change of stressing rate at any element i is a result of the initiation or termination of earthquake slip at element j and is given by:

$$\dot{\tau}_i = \dot{\tau}_i \pm K_{ij}^{\tau} \dot{\delta}_j^{EQ} \qquad (2.6)$$

$$\dot{\sigma}_i = \dot{\sigma}_i \pm K_{ij}^{\tau} \dot{\delta}_j^{EQ} \qquad \text{(no summation)} \qquad (2.7)$$

where the + and – refer to 1 → 2 and 2 → 0 transitions on element j, respectively. Hence, these state transition events require only one multiply and add operation at each element to update stressing rates everywhere in the model (no system-scale updates are required for the 0 → 1 transition). The changes to the stressing rates are applied instantaneously to all patches in the model (but note that the stresses themselves do not change discontinuously). Because the transition times depend only on initial conditions and stressing rates, computation proceeds in steps that mark the transition from one sliding state to the next without calculation of intermediate steps. This approach completely avoids computationally intensive solutions of systems of equations at closely spaced time intervals. Computation time for an earthquake event of some fixed size, embedded in a model with N fault elements, scales approximately by N^1. For example, a model with

40,000 fault elements that generates 500,000 earthquakes requires less than 24 hours on a single 2.5 GHz, G5 processor. Computational time increases by ~10x when fault creep is added.

Fault elements in regions that are modeled as creeping continuously have a rate-strengthening dependence of steady-state stress on slip speed ($b < a$ in equation (Eq. 2.3)). These elements are approximated as always being in steady-state creep and thus their slip speeds at any time are determined by the applied stresses from equation (Eq. 2.3) combined with $\theta_{ss} = D_c/\dot{\delta}$. Slip rates on these elements are approximated as piece-wise constant functions of time with updates when the deviation of the applied stresses from those used to set the current slip speed exceed a threshold.

For this study, stressing-rate boundary conditions drive fault slip and are determined by the back-slip method [*Savage,* 1983; *King and Bowman*, 2003]. With this method the stressing rates that act on individual fault elements are found through a one-time calculation, in which all fault elements slip backwards at specified long-term slip rates. This ensures that long-term stressing rates are consistent with observed slip rates. This method provides a combined representation of all external stressing sources, including tectonic stressing and stress transfer from off-fault yielding, consistent with prescribed/observed slip rates. A characteristic of back-slip stressing is that regions of uniform long-term slip rate require non-uniform stressing rates – stressing rates vary most strongly at the ends and bottom of the fault. A tectonic slip rate of 37 mm/yr is used for all studies, which is the average convergence rate of along the Cascadia Subduction Zone [*McCory et al.*, 2004].

Although the simulations employ approximations of the rupture process to achieve computational efficiency those approximations do not appear to seriously distort the model results, at least in the case of earthquakes. *Dieterich and Richards-Dinger* [2010] made a series of comparisons between seismic ruptures in RSQSim and those in fully dynamic 3D finite element codes. While some details of rupture propagation with RSQSim differ from results obtained with the fully dynamic codes, the simulations are remarkably similar in most respects, including rupture complexity. Because SSEs are modeled as slow earthquakes, the SSE simulations should have comparable computational accuracies, subject to our assumption of constant slip speed during an event. Although in the absence of a known physical mechanism for SSEs, a comparison cannot be made with dynamic models in the same manner as for earthquake ruptures.

The simulations reported here use values for two parameters that were tuned using the above mentioned finite element simulation comparisons. The first reduces parameter a (herein referred to as the a-reduction factor) at the rupture front where the stress concentration is poorly resolved because stresses are calculated at the center of each element. This is done when an element enters state 2, at which point the a-value on adjacent elements is multiplied by the a-reduction factor. An a-reduction factor of 0.10 is used here. The second adjustable parameter sets the stress (relative to the steady-state friction at the SSE or seismic slip speed) at which the slip terminates (herein referred to as the stress overshoot factor). During an earthquake if sliding stops at stresses that are sufficiently below the sliding friction, then healing outpaces re-stressing from continuing slip on adjacent regions of the fault. Such behavior inhibits renewed or continuing slip and leads to pulse-like ruptures. Conversely, if sliding stops at or only slightly below the sliding friction, then continuing slip on adjacent regions of the fault can immediately trigger renewed sliding before healing can occur. This effect favors on- and off switching of slip, which approximates continuous slip over broad regions at slow slip speeds. Such behavior is characteristic of crack-like rupture. Thus the stress overshoot factor affects the pulse-like versus crack-like characteristics of ruptures in RSQSim. A stress overshoot factor of 0.10 is used here, meaning that the stress at the cessation of slip is below the steady-state value (at the imposed slip speed) by 0.1 times the difference between that steady state value and the value at the onset of slip.

For this study I conducted sensitivity tests to determine the effect, if any, that the cell size, *a*-reduction factor, stress overshoot parameter, and slip speed may have on the rupture propagation speed of SSEs. These tests indicate: 1) the propagation speed is independent of the cell size, which is supported by the analytic solutions [*Colella et al.*, in review; Chapter 4]. 2) Small changes in the forward propagation speed (± 3 km/day) result from small changes in the *a*-reduction factor (± 50%), but there are no significant changes in back propagation speeds. 3) Changes in the stress overshoot parameter do not affect forward propagation speeds, however along-dip propagation speeds increase as the stress overshoot parameter decreases. Additionally, analytical solutions indicate that for very rapid along-dip speeds these speeds are sensitive to cell size [*Colella et al.*, in review; Chapter 4, equation 8). 4). Propagation speed is linearly proportional to changes in the slip speed. While the slip speed is a tunable parameter, laboratory experiments performed on Nankai decollement fault rock suggest a minimum (*a* - *b*) at a slip speed velocity of 10^{-6} m/s [*Ikari et al*., 2009; 2011].

2.3 References

Brune, J. (1970), Tectonic stress and the spectra of seismic shear waves from earthquakes. *J. Geophys. Res.*, *75*, 4997-5009.

Colella, H. V., J. H. Dieterich, K. B. Richards-Dinger (2011), Multi-event simulations of slow slip events for a Cascadia-like subduction zone, *Geophys. Res. Lett., 38*, L16312, doi:10.1029/2011GL048817.

Colella, H. V., J. H. Dieterich, K. B. Richards-Dinger, and A. Rubin, Complex characteristics of slow slip events reproduced in multi-cycle simulations, *submitted.*

Dieterich, J. H. (1979), Modeling of rock friction 1. Experimental results and constitutive equations, *J. Geophys. Res., 84*(B5), 2161 – 2168, doi:10.1029/JB084iB05p02161.

Dieterich, J. H. (1981), Constitutive properities of faults with simulated gouge, in Monograph 24, Mechanical behavior of crustal rocks, edited by N. L. Carter, M. Friedman, J. M. Logan, and D. W. Sterns, Am. Geophys. Union, Washington, D. C., 103-120.

Dieterich, J. H. (1995), Earthquake simulations with time-dependent nucleation and long-range interactions. *J. Nonlin. Proc. Geophys.*, **2**, 109–120 (1995).

Dieterich J. H., B. Kilgore (1996), Implications of fault constitutive properties for earthquake prediction, *Proceed. Nation. Acad. Sci., 93*, 3787–3794.

Dieterich, J. H., and K. Richards-Dinger (2010), Earthquake recurrence in simulated fault systems, *Pure Appl. Geophys.,* doi:10.1007/s00024-010-0094-0.

Ikari, M. J., and D. M. Saffer (2011), Comparison of frictional strength and velocity dependence between fault zones in the Nankai accretionary complex, *Geochem. Geophys. Geosyst., 12*, Q0AD11, doi:10.1029/2010GC003442.

Ikari, M. J., D. M. Saffer, and C. Marone (2009), Frictional and hydrologic properties of a major splay fault system, Nankai subduction zone, *Geophys. Res. Lett., 36*, L20313, doi: 10.1029/2009GL040009.

King, G. C. P., and D. D. Bowman (2003), The evolution of regional seismicity between large earthquakes, *J. Geophys. Res., 108*, doi:10.1029/2001JB000783.

Linker, M. F., and J. H. Dieterich (1992), Effects of variable normal stress on rock friction – Observations and constitutive equations, *J. Geophys. Res., 97*, 4923-4940.

Liu, Y., and J. R. Rice (2005), Aseismic slip transients emerge spontaneously in three-dimensional rate and state modeling of subduction earthquake sequences, *J. Geophys. Res., 110*, B08307, doi:10.1029/ 2004JB003424.

Liu, Y., and J. R. Rice (2007), Spontaneous and triggered aseismic deformation transients in a subduction fault model, *J. Geophys. Res., 112*, B09404, doi:10.1029/2007JB004930.

McCrory, P. A., J. L. Blair, D. H. Oppenheimer, and S. R. Walter (2004), Depth to the Juan de Fuca slab beneath the Cascadia subduction margin: A 3-D model for sorting earthquakes, *U.S.G.S. Data Series DS-91*, 1 CD-ROM, version 1.2.

Okada, Y. (1992), Internal deformation due to shear and tensile faults in a half-space, *Bull. Seismol. Soc. Am., 82*(2), 1018– 1040.

Peacock, S. M., K. Wang, and A. M. McMahon (2002), Thermal structure and metamorphism of subducting oceanic crust: Insight into Cascadia intraslab earthquakes, *in The Cascadia Subduction Zone and Related Subduction Systems: Seismic Structure, Intraslab Earthquakes and Processes, and Earthquake Harzards*, edited by S. Kirby, K. Wang, and S. Dunlop, U.S. Geol. Surv. Open File Rep., 02-328, 123– 126.

Rice, J. R. (1983), Constitutive relations from fault slip and earthquake instabilities*, Pure Appl. Geophys., 121*, 443-475, doi:10.1007/BF02590151.

Rubin, A. M. (2008), Episodic slow slip events and rate-and-state friction, *J. Geophys. Res., 113*, B11414, doi:10.1029/2008JB005642.

Rubin, A. M. (2011), Designer friction laws for bimodal slow slip propagation speeds, *Geochem. Geophys. Geosyst.*, *12*, Q04007, doi:10.1029/2010GC003386.

Ruina, A. L. (1983), Slip instability and state variable friction laws, *J. Geophys. Res., 88*(B12), 10,359 – 10,370, doi:10.1029/JB088iB12p10359.

Savage, J. C. (1983), A dislocation model of strain accumulation and release at a subduction zone, *J. Geophys. Res., 88*, 4984-4996.

Shibazaki, B., and Y. Iio (2003), On the physical mechanism of silent slip events along the deeper part of the seismogenic zone, *Geophys. Res. Lett., 30*(9), 1489, doi: 10.1029/2003GL017047.

Tse, S. T., and J. R. Rice (1986), Crustal earthquake instability in relation to the depth variation of frictional slip properties, *J. Geophys. Res., 91*(B9), 9452– 9472, doi:10.1029/JB091iB09p09452.

Chapter 3

Multi-event simulations of slow slip events for a Cascadia-like subduction zone

Originally published in *Geophysical Research Letters*

Colella, H. V., J. H. Dieterich, K. B. Richards-Dinger (2011), Multi-event simulations of slow slip events for a Cascadia-like subudction zone, *Geophys. Res. Lett.*, *38*, L16312, doi:10.10229/2011GL0488141.

Abstract.

We employ the earthquake simulator, RSQSim, which incorporates rate- and state-dependent friction, to investigate characteristics of slow slip events (SSEs) along a Cascadia-like megathrust. The simulations consist of 100,000 SSEs with equivalent moment magnitudes M_w 4.0-7.0. The largest simulated SSEs (M_w 6.4-7.0) have inter-event times of ~19 months, durations of 10-40 days, mean slips of 2.2-4.1 cm, and along-strike propagation speeds of 7-20 km/day, which are comparable to observations from Cascadia. The simulations show quiescence after $M_w > 6.4$ SSEs, followed by a progressive increase in both the magnitude and frequency of SSEs prior to the next large event. Small SSEs, below ~M_w5.6, develop in an incoherent manner and have irregular geometries, while larger SSEs show highly coherent growth of the slip region and spontaneous, but transient, event-to-event segmentation. The change in event characteristics at ~M_w5.6 corresponds to a break in the scaling of seismic moment with slip, fault area, and duration.

3.1 Introduction

Episodic slow slip events (SSEs), typically lasting a few days to weeks and recurring at regular intervals, have been detected along several subduction zones worldwide [*Hirose et al.*, 1999; *Dragert et al*., 2001; *Lowry et al*., 2001; *Kostoglodov et al.*, 2003; *Douglas et al.*, 2005; *Ohta et al.*, 2006]. Geodetic inversions indicate Cascadia SSEs occur adjacent to and down-dip of the seismogenic portion of the mega-thrust in what has been inferred to represent a transition zone between sections of the subduction interface that slip in earthquakes and sections that slip continuously by fault creep [*Dragert et al.,* 2004]. In the following we report initial results from a new multi-event simulation method that permits the study of long histories of SSEs, their scaling characteristics, and interactions between SSEs and adjacent fault sections.

3.2 Model

The simulations incorporate rate- and state-dependent fault constitutive properties for the sliding strength of faults [*Dieterich*, 1979; 1981, *Ruina*, 1983; *Rice*, 1983] as represented by the following equations:

$$\tau = \sigma\left[\mu_0 + a\ln\left(\frac{\dot{\delta}}{\dot{\delta}^*}\right) + b\ln\left(\frac{\theta}{\theta^*}\right)\right] \tag{3.1}$$

$$d\theta = dt - \frac{\theta}{D_c}d\delta - \frac{\alpha\theta}{b\sigma}d\sigma \tag{3.2}$$

where τ and σ are the shear and normal stress, respectively, acting on a fault element during slip, μ_0 is the nominal coefficient of friction, a and b are experimentally determined constants with values that generally range from 0.008-0.015; $\dot{\delta}$ is sliding speed; θ is a state variable that evolves with time, normal stress, and over a characteristic slip distance D_c; and $\dot{\delta}^*$ and θ^* are normalizing constants. The evolution of θ in (1) incorporates the effects of normal stress changes on θ (where α =0.25 in these simulations) [*Linker and Dieterich*, 1992]. A necessary condition for unstable earthquake slip is $(b - a) > 0$, wherein the fault weakens with increasing slip speed (rate-weakening) during steady-state slip. Conversely, if $(b - a) < 0$ steady-state friction increases with slip speed (rate-strengthening) and the mode of slip is that of continuous, stable fault creep.

Previous modeling studies of SSEs employ rate- and state-dependent constitutive laws, and largely focus on possible mechanisms that quench the acceleration of slip during the nucleation process of SSEs before earthquake slip speeds are reached. *Shibazaki and Iio* [2003] use a variant of rate-state friction that gives rate-weakening at slow slip speeds and rate-strengthening at high slip speeds to limit the sliding speed. *Liu and Rice* [2005; 2007] and *Rubin* [2008] show that SSEs can arise under a narrow range of conditions near the boundary between stable and unstable slip, namely small positive values of $(b - a)$ in combination with low effective normal stress. This class of models requires a sufficiently high system stiffness, which scales inversely with the width of the transition zone, to prevent runaway slip speeds. *Segall et al.* [2010] demonstrate that pore-fluid interactions lead to dilatant strengthening that may stabilize slip in SSEs before seismic slip speeds are reached. These modeling studies demonstrate the plausibility of three very different mechanisms for controlling slip speed in SSEs. However, which of those mechanisms, if any, underlie SSEs remains uncertain.

In this study we take a different approach – one that does not address the unknown factors that control slip speed in SSEs, but focuses on modeling possible observables such as slip-per-event, inter-event times, scaling relations, and propagation speeds. In essence we model SSEs as slow earthquakes, wherein the slip speed during a SSE is specified as an input parameter based on observations, rather than an outcome of the calculations – otherwise the simulations are fully deterministic in the nucleation location and time, propagation speed, event duration, and final distribution of slip.

To implement the model we use the simulation code Rate-State-Quake-Simulator (RSQSim) [*Dieterich and Richards-Dinger*, 2010]. RSQSim is a boundary element code capable of modeling earthquake slip, slow slip, and continuous creep; and it is computationally efficient, which permits long histories with a wide range of event sizes. The simulations fully incorporate 3D elastic stress interactions, which include the effects of normal stress fluctuations on sliding friction, and it accepts complex fault geometries. The code employs event-driven computational steps, where the evolution of conditions between steps is given by approximate analytic solutions for computational efficiency. For more details on RSQSim, see Chapter 2, Section 2.2. SSEs are modeled in the same way as earthquakes, but with slower slip speeds. Slip rates along creeping sections of faults are updated as stresses evolve due to elastic interactions, assuming steady-state friction.

In the simulations SSEs spontaneously nucleate as given by the analytic solutions of *Dieterich* [1992; 2007] and *Fang et al.* [2010]. Laboratory experiments [*Dieterich and Kilgore*, 1996] and detailed numerical calculations [*Dieterich,* 1992; *Fang et al.*, 2010] demonstrate that those solutions accurately capture the time- and stress-dependence of the acceleration of slip during transition from an essentially locked state to more rapid slip in an event. Because RSQSim employs a quasi-static assumption, the processes that control SSE rupture propagation are identical to those at higher slip speeds in earthquakes. The rupture calculations have been validated and calibrated by comparisons with detailed, fully dynamic finite element rupture simulations [*Dieterich and Richards-Dinger*, 2010]. The simulations reported below use values for two parameters that were tuned using finite element simulations. The first reduces parameter *a* at the rupture front where the stress concentration is poorly resolved (*a*-reduction factor = 0.1); and the second sets the stress relative to sliding friction at the termination of slip (stress overshoot factor = 0.1). Initial tests indicate that simulation results for SSEs presented here are insensitive to changes in these parameters. The tests also indicate that SSE propagation speeds are independent of cell size.

The models use a Cascadia-type configuration, where the mega-thrust is divided into three sections based on their sliding characteristics: a seismogenic zone, a transition zone, and continuous creep zone (Figure 3.1). The seismogenic zone is located between depths of 5 and 25 km and corresponds to the section of the mega-thrust that generates great earthquakes. In this study simulations span a period of ~130 years, which is relatively short compared to the ~600 yr recurrence interval for great Cascadia earthquakes [*Goldfinger et al.,* 2003]. Hence, for simplicity, the seismogenic zone is held locked. The transition zone is located at depths of 25 km and 35 km and corresponds to the portion of the mega-thrust that experiences SSEs. The continuous creep zone is located at depths > 35 km and corresponds to stable sliding down-dip of the transition zone.

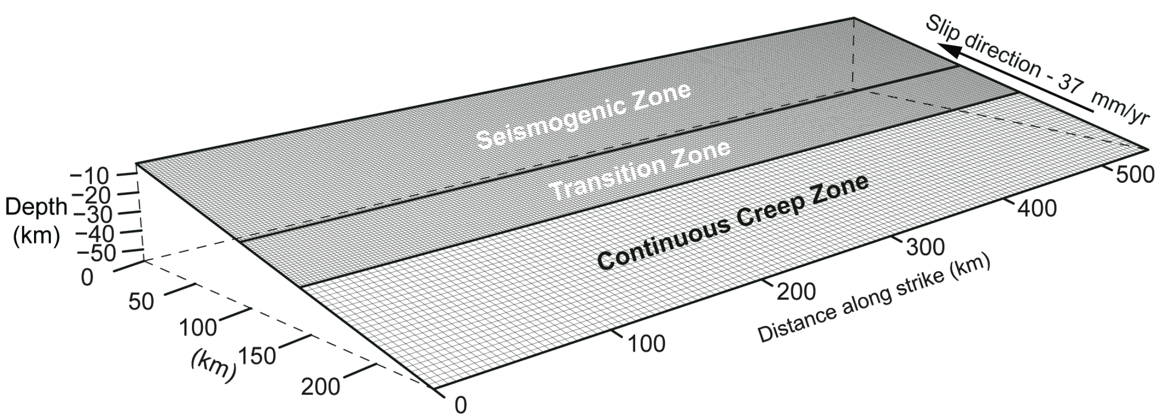

Figure 3.1. *Model of a subduction mega-thrust. The fault is 552 km x 246 km and dips 12°. Fault elements are 2 km x 2 km in the seismogenic and transition zones and 4 km x 4 km in the continuous creep zone. Total number of fault elements is 23,598.*

Small positive values of (b - a) are expected in the transition zone between the seismogenic and creeping sections; and low effective normal stresses (σ) from dehydration reactions are indicated by thermal modeling [*Peacock et al.*, 2002] and seismological observations [*Kodaira et al., 2004*; *Shelly et al.*, 2006]. Based on these considerations the simulations use σ = 4.5 MPa and ($b - a$) = 0.002, with uniform b- and a-values of 0.012 and 0.010, respectively, in the transition zone. The simulations use σ =

4.5 MPa and $(b - a) = -0.002$, with uniform b and a-values of 0.008 and 0.010, respectively, in the continuous creep zone. Additionally we assign $D_c = 10^{-5}$ m and Lame´ elastic parameters $\lambda = \mu = 30$ GPa. The results reported here use a SSE slip speed of 1.25 x 10^{-6} m/s. This value, together with the assumed values of a, b and σ, yield SSEs that agree rather well with observations for Cascadia, including inferences of SSEs from tectonic tremor observations. Fault slip is driven by stressing-rate boundary conditions derived from the back-slip method [*Savage*, 1983; *King and Bowman*; 2003], with a tectonic slip rate of 37 mm/year. Slip does not occur outside the limits of the model.

3.3 Results

The simulations consist of 100,000 SSEs with moment magnitudes that range from ~M_w4.0 to ~M_w7.0. The simulations reach a statistical equilibrium following a run-up time of ~10 years (run-up data are excluded from reported results). Because SSEs may penetrate into and hence interact with the adjacent continuous creep zone, simulations both with and without a creeping zone are used to explore these effects.

Figure 3.2 illustrates several characteristics of simulated SSEs. 1) Different regions of the model often slip simultaneously, which results in overlapping rupture times. This effect is observed in both small and large SSEs. 2) Small SSEs ($M_w \leq 5.6$) and the first few days of larger SSEs are usually quite incoherent with irregular geometries, and could be described as swarms of smaller sub-events, which contain time intervals where slip is locally interrupted (Figure 3.2a). 3) For large events ($M_w > 5.6$) the initial incoherent interval is followed by highly coherent propagation with a sharply defined rupture front that propagates at speeds ranging from 7-20 km/day (Figure 3.2a & 3.2b). 4) Large SSEs that initiate at different locations often coalesce. 5) The termination phase of large SSEs often consists of decaying incoherent swarms of sub-events (Figure 3.2a). Because of these highly complex characteristics a precise definition of what constitutes the extent, beginning, and end of a SSE is quite problematic. Here a SSE is defined as the unbroken time interval during which slip occurs somewhere in the model. Consequently, a single event by this definition may include several discontinuous regions of slip.

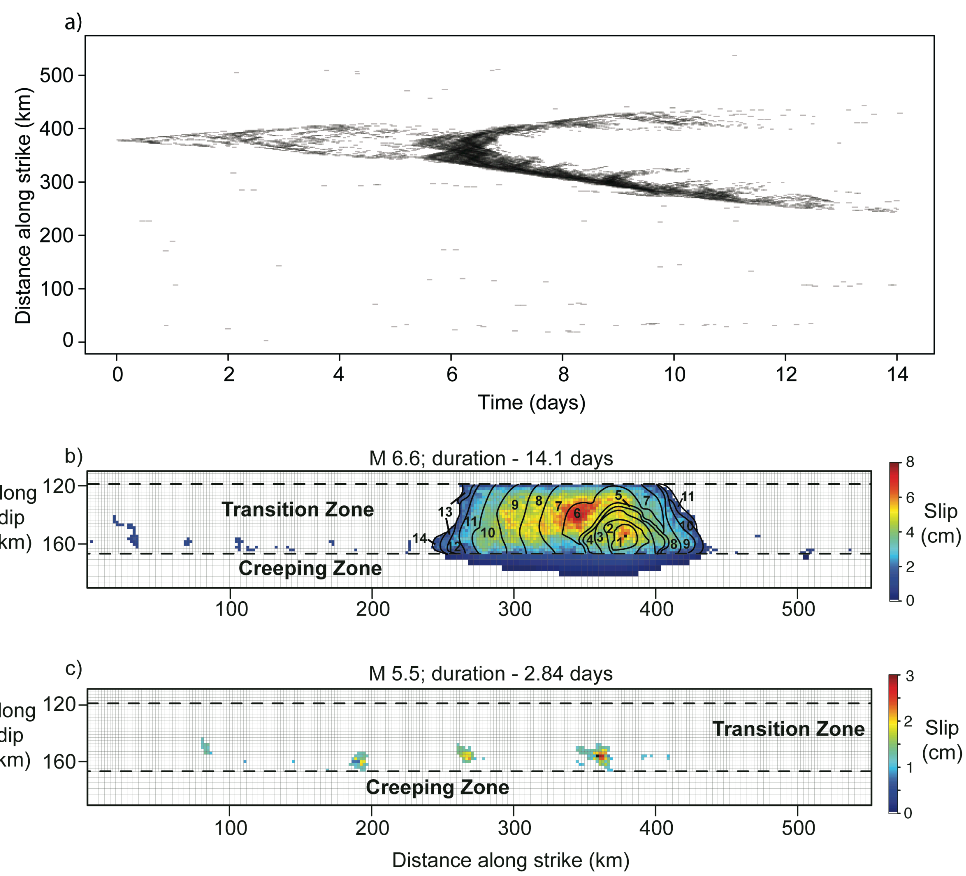

Figure 3.2: *a) Space-time evolution of slip during a simulated SSE. b) Final slip distribution for the event in a. Black contours map the progression of the rupture front in days. c). Slip distribution for a small SSE.*

The largest SSEs (M_w6.4-7.0) typically initiate near the bottom of the transition zone and then propagate along strike (Figure 3.2b). The average event duration and slip for these events are ~14 days and ~3.6 cm, respectively. Similar event durations and slip are observed along the Cascadia Subduction Zone [*Miller et al.,* 2001; *Dragert et al.,* 2004]. In Figure 3.2b also note the penetration of slip into the continuous creep zone.

Figure 3.3 summarizes source parameters from the simulations. Moment magnitude-frequency distributions show power-law scaling up to ~M_w5.6 with b-values of 1.63 and 1.44 for simulations with and without continuous creep, respectively, and a tail to the distributions that suggests a characteristic event magnitude at ~M_w6.7 (Figure 3.3a). The ~M_w5.6 scaling break, which appears to be associated with the transition from incoherent to coherent rupture growth, is discussed below. Rupture lengths of the largest events (M_w~7.0) approach the entire length of the model. Simulations without continuous creep have more abundant moderate-sized events compared to models with continuous creep, which is reflected in the lower b-value. Inter-event times of the largest SSEs are ~19 months for simulations with continuous creep and ~10 months for simulations without continuous creep.

Figure 3.3b shows a plot of mean slip against equivalent seismic moment. Slip is nearly independent of seismic moment for $M_w < 5.6$. Slip increases with seismic moment for $M_w \geq 5.6$ with approximate scaling of $M_0 \propto \delta^3$, where δ represents slip. The near independence of mean slip on seismic moment below the scaling break appears to reflect the incoherent behavior of small events, wherein the sub-events have similar slip. The δ^3

scaling for $M_w \geq 5.6$ is consistent with the observed coherent rupture growth assuming self-similar 2D expansion of ruptures. As the magnitude of a SSE increases, penetration of slip into the creeping zone also increases, which allows progressively larger displacements in the transition zone relative to the simulation without continuous creep. The average displacement is ~16% greater in the simulation with continuous creep for M_w6.7-6.9.

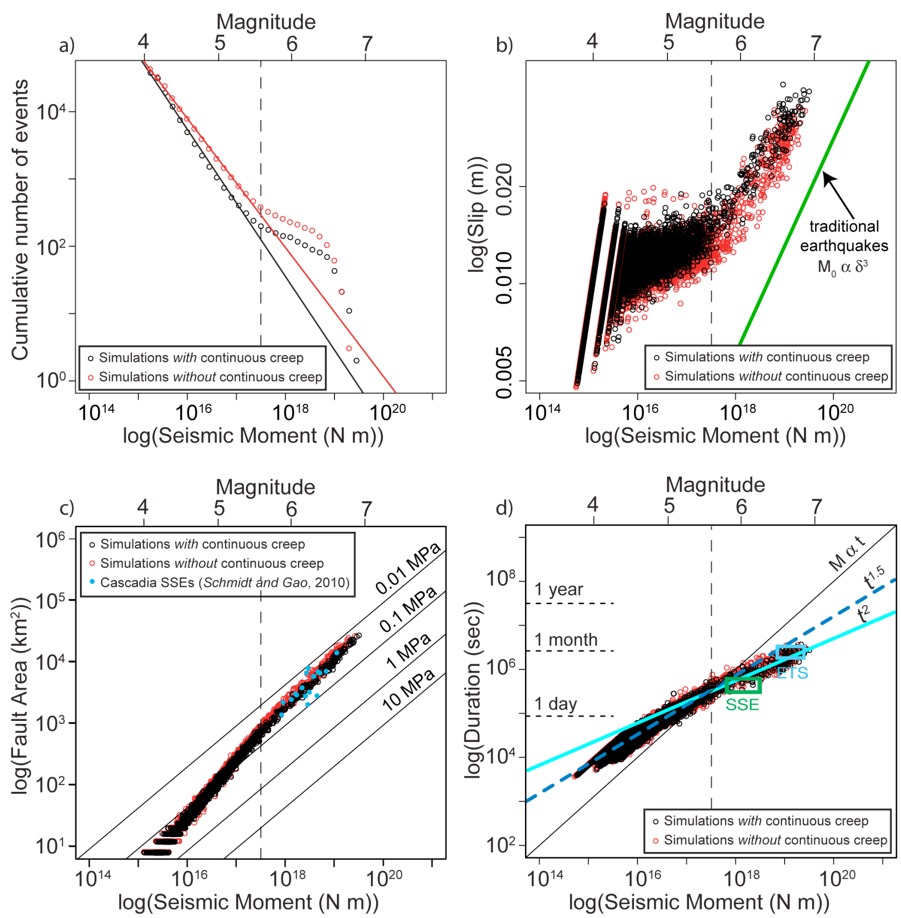

Figure 3.3 *a) Seismic moment-cumulative frequency distribution. Black and red lines are best-fits for M_w<5.6 in simulations with and without a continuous creep zone, respectively. b) Seismic moment versus mean SSE slip (excluding slip occurring in the creeping section). c) Seismic moment versus fault area in the transition zone (excluding slip in creeping zone). Diagonal lines contour constant static stress drop for a circular crack [Kanamori and Anderson, 1975]. d) Seismic moment versus duration. Blue and green rectangles are SSEs reported for Cascadia and Nankai, respectively [Ide et al., 2007]. The black dotted line represents the scaling break at ~M_w5.6.*

The dependencies of fault area and event duration on seismic moment are shown in Figures 3.3c and 3.3d, respectively. Above $M_w \geq 5.6$ the fault area-seismic moment scaling roughly follows constant stress drop, which is consistent with 2D self-similar growth of event area inferred from slip data. The largest SSEs have a ~16% smaller stress drop in the simulation without an adjacent continuous creep zone, a consequence of a smaller average slip per event. The seismic moment versus event duration results indicate $M_0 \propto t^2$ for SSEs $M_w \geq 5.6$ and $M_0 \propto t^{1.5}$ for SSEs $M_w < 5.6$. Data for Cascadia SSEs from *Schmidt and Gao* [2010] and for Cascadia and Nankai SSEs from *Ide et al.* [2007] are plotted for comparisons with simulations.

Figure 3.4 illustrates space-time characteristics of simulated SSEs. First, the occurrence rate of small and moderate SSEs is modulated by the largest events (Figure 3.4a & 3.4b). Specifically, rates of smaller events increase prior to the largest SSEs, followed by an interval of quiescence. A similar pattern is observed in tremor swarms in Cascadia [*Wech et al*., 2010], which are considered proxies for SSEs [*Gomberg*, 2010, and aforementioned summaries]. Second, there are patterns of spontaneous, but transient, segmentation of large SSEs, which consist of regular patterns of repeated failures along similar sections of the fault that change through time (Figure 3.4c). Rarely does the whole transition zone slip in a single event; instead it slips in segments that result in $M_w > 6.4$ SSEs every ~19 months. Such a sequence persists for several cycles before evolving to a new pattern. The addition of mechanical heterogeneities may create more persistent patterns. Third, as previously stated, simulated SSEs often consist of non-contiguous slip patches (e.g. Event 1, 2 and 4).

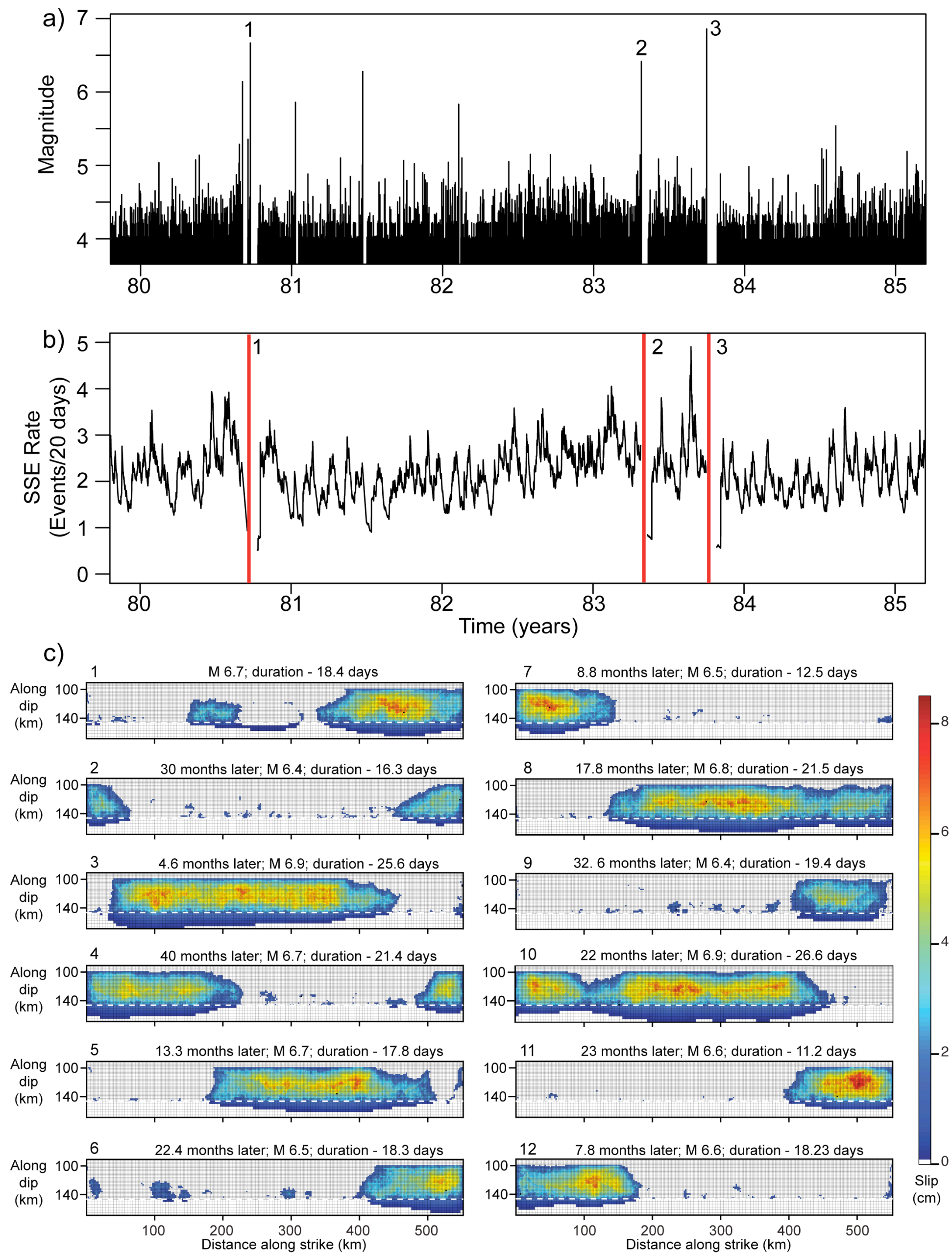

Figure 3.4. *Space-time characteristics of simulated SSEs. a). Magnitude versus time (model with continuous creep). b). SSEs-per-20 days for the period shown in a). c). Slip distribution for a 22-yr sequence of M_w>6.4 SSEs, where events 1-3 correspond to those in a) and b). Note the penetration of slip into the continuous creep zone.*

3.4 Discussion

In summary, the simulations broadly agree with a wide range of characteristics of SSEs reported for Cascadia. The largest simulated SSEs (M_w6.4-7.0) have mean slip of 2.2-4.1 cm compared to 2.3-4.0 cm, and durations of 10-40 days compared to 10-35 days, for Cascadia [*Dragert et al.*, 2004]. Simulated rupture propagation speeds are 7-20 km/day compared to 6-18 km/day reported by *Dragert et al.* [2004]. We also see rapid back-propagation effects similar to those reported by *Houston et al.* [2011], which will be addressed in a forthcoming paper. Seismic moment-fault area and seismic moment-event duration relationships for the largest events are also consistent with those for Cascadia and Nankai (Figure 3.3c-d). Additionally, the simulations show a progressive increase in magnitude and frequency of SSEs prior to $M_w > 6.4$ events, followed by a period of quiescence, similar to the pattern observed in tremor swarms reported by *Wech et al.* [2010]. We note that large SSEs lack robust Omori-type temporal clustering characteristics of earthquake aftershocks, although RSQSim reproduces those effects with earthquake simulations [*Dieterich and Richards-Dinger,* 2010]. To date no such clustering has been reported for SSEs. Finally, simulated SSEs often occur simultaneously at several locations including events that occasionally coalesce. A similar effect of overlapping slip times and event convergence is observed in large Cascadia SSEs [*Boyarko and Brudzinski*, 2010] and is quite evident in the space-time plots of tremor reported by *Wech et al.* [2010].

A persistent feature of the simulations is the change from incoherent development of SSEs to coherent rupture growth at ~M_w5.6, which is associated with the break in the scaling relationships shown in Figure 3.3. The magnitude at which the scaling break occurs may be sensitive to model parameters, but that has not yet been explored. Simulated SSEs also have indistinct initiation and termination and overlapping rupture times in different regions. These characteristics make it rather difficult to precisely define what constitutes a SSE in simulations and perhaps in nature as well. Hence, the scaling break may change with the definition of a SSE.

A possible departure of simulated SSEs from observed SSEs is the seismic moment-duration scaling. The simulations yield $M_0 \propto t^{\sim 1.5}$ for events $M_w < 5.6$, and $M_0 \propto t^{\sim 2}$ for events $M_w \geq 5.6$ (Figure 3.3d), while *Ide et al.* [2007] propose a linear scaling ($M_0 \propto t$) based on a synthesis of data from different regions. However, *Peng and Gomberg* [2010] conclude that the seismic moment-duration scaling relationship may not be as simple as originally proposed. This is supported by observations of *Ide et al.* [2008], which indicate the best-fit scaling for a set of slow earthquakes from Kii Peninsula in western Japan that last 20-200s and are estimated to be M_w3-4, is $M_0 \propto t^{1.5}$ and *Gao et al.* [*Gao et al.,* manuscript in preparation, 2011], which indicate $M_0 \propto t^{1.1-1.7}$ based on geodetic observations for Cascadia SSEs with moment magnitudes that range from M_w6.4-6.9.

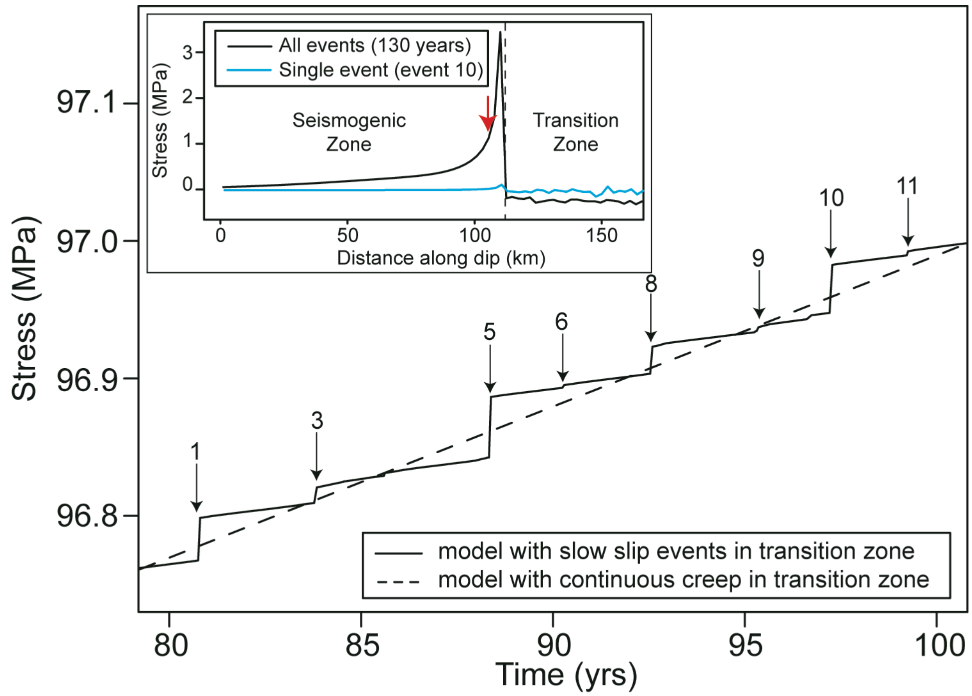

Figure 3.5. *Shear stress 6 km (up-dip distance) from the base of the seismogenic zone (red arrow) is given by the solid black curve. Black arrows correspond to numbered events in Figure 3.4. Inset shows shear stress transfer to the seismogenic zone following a single event (cyan curve) and 130 years of SSEs (black curve).*

Stress transfer during SSEs strongly affects stressing rates in the seismogenic zone (Figure 3.5) and may directly affect the occurrence of great subduction earthquakes [*Mazzotti and Adams*, 2004]. Our simulation approach provides a means to investigate the interactions between SSEs and adjacent sections of the subduction interface. The stressing rate near the base of the seismogenic zone is 0.005 MPa/yr in the interval between SSEs compared to a maximum rate of ~0.67 MPa/yr during a large SSE. Over time this stress transfer results in elevated stress levels near the base of the seismogenic zone (Figure 3.5, inset), which may favor 1) an increase of seismicity along the base of the seismogenic zone and 2) enhanced probabilities of nucleation of the next great earthquake associated with the occurrence of a SSE. In addition, just as slip during a SSE penetrates into the creeping zone, we expect slip during a great earthquake to penetrate into the transition zone. This may have important implications with respect to the down-dip extent of subduction earthquakes and modulation of SSE activity by great earthquakes. We plan to implement mega-thrust earthquakes in the simulations to investigate these questions.

3.5 References

Boyarko, D. C. and M. R. Brudzinski (2010), Spatial and temporal patterns of nonvolcanic tremor along the southern Cascadia subduction zone, *J. Geophys. Res., 115*, B00A22, doi:10.1029/2008JB006064.

Dieterich, J. H. (1979), Modeling of rock friction 1. Experimental results and constitutive equations, *J. Geophys. Res., 84*, 2161-2168.

Dieterich, J. H. (1981), Constitutive properities of faults with simulated gouge, in Monograph 24, Mechanical behavior of crustal rocks, edited by N. L. Carter, M. Friedman, J. M. Logan, and D. W. Sterns, Am. Geophys. Union, Washington, D. C., 103-120.

Dieterich, J. H. (1992), Earthquake nucleation on faults with rate- and state-dependent strength, *Tectonophysics*, *211*, 115–134.

Dieterich J. H., Kilgore B. (1996), Implications of fault constitutive properties for earthquake prediction, *Proceed. Nation. Acad. Sci., 93*, 3787–3794.

Dieterich, J. H., and K. Richards-Dinger (2010), Earthquake recurrence in simulated fault systems, *Pure Appl. Geophys.,* doi:10.1007/s00024-010-0094-0.

Douglas, A., J. Beavan, L. Wallace, J. Townend (2005), Slow slip on the northern Hikurangi subduction interface, New Zealand, *Geophys. Res. Lett., 32*, L16305, doi: 10.1029/2005GL023607.

Dragert, H., K. Wang, and T. S. James (2001), A silent slip event on the deeper Cascadia subduction interface, *Science, 292*, 1525-1528, doi:10.1126/science.1060152.

Dragert, H., K. Wang, and G. Rogers (2004), Geodetic and seismic signatures of episodic tremor and slip in northern Cascadia subduction zone, *Earth Planets Space*, 56, 1143-1150.

Fang, Z., J. H. Dieterich, G. Xu, Effect of initial conditions and loading path on earthquake nucleation, *J. Geophys. Res., 115*, doi:10.1029/2009JB006558, 2010.

Goldfinger, C., C. H. Nelson, J. E. Johnson (2003), Holocene earthquake records from the Cascadia Subduction Zone and northern San Andreas Fault based on precise dating of offshore turbidites, *Annu. Rev. Earth. Planet. Sci., 31*, 55-577, doi:10.1146/annurev.earth. 31.100901.141246.

Gomberg, J. (2010), Introduction to special section on phenomenology, underlying processes, and hazard implications of aseismic slip and nonvolcanic tremor, *J. Geophys. Res., 115*, B001A00, doi:10.1029/2010JB008052.

Hirose, H., K. Hirahara, F. Kimata, N. Fuji, and S. Miyazaki (1999), A slow thrust slip event following the two 1996 Hyuganada earthquakes, *Geophys. Res. Lett.*, *26,* 3237-3240, doi:10.1029/1999GL010999.

Houston, H., B. G. Delbridge, A. G. Wech, and K. C. Creager (2011), Rapid tremor reversals in Cascadia generated by a weakened plate interface, *Nature Geosci., 4*, 404-409, doi:10.1028/ngeo1157.

Ide, S., G. C. Beroza, D. R. Shelly, and T. Uchide (2007), A scaling law for slow earthquakes, *Nature*, *447,* 76-79, doi:10.1038/nature05780.

Ide, S., K. Imanishi, Y. Yoshida, G. C. Beroza, and D. R. Shelly (2008), Bridging the gap between seismically and geodetically detected slow earthquakes, *Geophys. Res. Lett., 35*, L10305, doi:10.1029/2008GL034014.

Kanamori, H. and D. L. Anderson (1975), Theoretical basis of some empirical relations in seismology, *Bull. Seismol. Soc. Am., 65*, 1073-1095.

King, G. C. P., and D. D. Bowman (2003), The evolution of regional seismicity between large earthquakes, *J. Geophys. Res., 108*, doi:10.1029/2001JB000783.

Kodaira, S., T. Iidaka, A. Kato, J. O. Park, T. Iwasaki, Y. Kaneda (2004), High pore fluid pressure may cause silent slip in the Nankai trough, *Science, 304*, 1295-1298, doi: 10.1016/science.1096535.

Kostoglodov, V., S. K. Singh, J. A. Santiago, K. M. Larson, A. R. Lowry, and R. Bilham (2003), A large silent earthquake in the Guerrero seismic gap, Mexico, *Geophys. Res. Lett., 30(15)*, 1807, doi:10.1029/2003GL017219.

Linker, M.F., and J.H. Dieterich (1992), Effects of variable normal stress on rock friction – Observations and constitutive equations, *J. Geophys. Res., 97*, 4923-4940.

Liu, Y., and J. R. Rice (2005), Aseismic slip transients emerge spontaneously in three-dimensional rate and state modeling of subduction earthquake sequences, *J. Geophys. Res., 110*, B08307, doi:10.1029/2004JB003424.

Liu, Y., and J. R. Rice (2007), Spontaneous and triggered asesimic deformation transients in a subduction fault model, *J. Geophys. Res., 112*, B09404, doi:10.1029/2007JB004930.

Lowry, A.R., K.M. Larson, V. Kostoglodov, and R. Bilham, Transient fault slip in Guerrero, southern Mexico (2001), *Geophys. Res. Lett.*, *28,* 3753-3756, doi: 10.1029/2001GL013238.

Mazzotti, S., and J. Adams (2004), Variability of near-term probability for the next great earthquake on the Cascadia Subduction Zone, *Bull. Seismol. Soc. Am., 94*, 1954-1959.

Miller, M. M., T. Melbourne, D. J. Johnson, W. Q. Sumner (2001), Periodic slow earthquakes from the Cascadia subduction zone, *Science*, *295*, 2423.

Ohta, Y., Freymueller, J. T., Hreinsdottir, S., and Suito, H. (2006), A large slow slip event and the depth of the seismogenic zone in the south central Alaska subduction zone, *Earth Planet. Sci. Lett., 247*, 108-116, doi:10.1016/epsl.2006.05.013.

Peacock, S. M., K. Wang, and A. M. McMahon (2002), Thermal structure and metamorphism of subducting oceanic crust: Insight into Cascadia intraslab earthquakes, in *The Cascadia Subduction Zone and Related Subduction Systems: Seismic Structure, Intraslab Earthquakes and Processes, and Earthquake Hazards*, edited by S. Kirby, K. Wang, and S. Dunlop, *U.S. Geol. Surv. Open File Rep.*, *02-328*, 123-126.

Peng, Z., and J. Gomberg (2010), A integrated persepctive of the continuum between earthquakes and slow-slip phenomena, *Nature Geosience, 3*, doi:10.1038/NGEO0940.

Rice, J. R. (1983), Constitutive relations from fault slip and earthquake instabilities*, Pure Appl. Geophys., 121*, 443-475, doi:10.1007/BF02590151.

Rubin, A. M. (2008), Episodic slow slip events and rate-and-state friction, *J. Geophys. Res., 113*, B11414, doi:10.1029/2008JB005642.

Rubin, A. M. and J-P. Ampuero (2005), Earthquake nucleation on (aging) rate and state faults, *J. Geophys. Res., 110*, B11312, doi:10.1029/2005JB003686.

Ruina, A. (1983), Slip instability and state variable friction laws, *J. Geophys. Res., 88*, 10359-10370.

Savage, J. C. (1983), A dislocation model of strain accumulation and release at a subduction zone, *J. Geophys. Res., 88*, 4984-4996.

Segall, P., A. M. Rubin, A. M. Bradley, and J. R. Rice (2010), Dilatant strengthening as a mechanism for slow slip events, *J. Geophys. Res., 115*, B12305, doi: 10.1029/2010JB007499.

Schmidt, D. A. and H. Gao (2010), Source parameters and time-dependent slip distribution of slow slip events on the Cascadia subduction zone from 1998 to 2008, *J. Geophys. Res., 115*, B00A18, doi:10.1029/2008JB006045.

Shelly, D. R., G. C. Beroza, S. Ide, and S. Nakamula (2006), Low-frequency earthquakes in Shikoku, Japan, and their relationship to episodic tremor and slip, *Nature, 442*, 188-191, doi:10.1028/nature04931.

Shibazaki, N., and Y. Iio (2003), On the physical mechanism of silent slip events along the deeper part of the seismogenic zone, *Geophys. Res. Lett., 30*, 1489, doi: 10.1029/2003GL017047.

Wech, A. G., K. C. Creager, H. Houston., J. E. Vidale (2010), An earthquake-like magnitude-frequency distribution of slow slip in northern Cascadia, *Geophys. Res. Lett.*, *37*, L22310, doi:10.1029/2010GL04488.

Chapter 4

Complex characteristics of slow slip events reproduced in multi-cycle simulations

Science, in review

Abstract.

Since the discovery of slow slip events along subduction zone interfaces worldwide, dense geodetic and seismic networks have illuminated detailed characteristics of these events and associated tremor. High-resolution observations of tremor, whose spatial-temporal evolution is presumed to reflect that of the underlying slow slip events, show highly complex patterns whose origins remain poorly understood. We present a new, computationally efficient modeling technique that reproduces many features of observed slow slip events, including slow initiation, coalescence of separate events, and rapid back-propagation of renewed slip over previously slipped regions. Rapid back propagation speeds are explained as a consequence of rate- and state-dependent frictional healing, consistent with analytical solutions developed in support of the simulations.

Recent geodetic observations in subduction zones have revealed the widespread occurrence of intermittent strain release in the form of slow slip events (SSEs) along the subduction interface [e.g. *Schwartz and Rokosky*, 2007]. In Cascadia, which is the basis of the simulations presented here, SSEs typically have durations of 1-4 weeks, with 2-4 cm of slip, and occur every 9-21 months [*Dragert et al.,* 2002]. In the well-instrumented Shikoku and Cascadia subduction zones, slow slip is always accompanied by low-level tectonic tremor, which indicates that tremor observations can be used as a proxy for slip [*Miller et al.,* 2002; *Obara et al*., 2004; *Aguiar et al*., 2009]. High-resolution tremor observations indicate highly complex space-time patterns, which include slow, incoherent initiation and termination of events and simultaneous slip in multiple locations [*Boyarko and Brudzinski*, 2010; *Obara*, 2010]. Forward propagation speeds range from 5-18 km/day [*Dragert et al.,* 2002; *Miller et al.,* 2002; *Obara et al*., 2004; *Aguiar et al*., 2009; *Boyarko and Brudzinski*, 2010; *Obara*, 2010], while back propagation speeds and along-dip propagation speeds across previously slipped areas range from 100-300 km/day [*Houston et al*., 2011] to 24-4000 km/day [*Shelly et al.*, 2007; *Ghosh et al.,* 2010; 2011], respectively. Although various processes have been proposed that may influence these complex patterns, neither a physical mechanism nor a quantitative model has been agreed upon [*Ando et al.*, 2009; *Houston et al.,* 2010; *Ghosh et al.,* 2010; 2011; *Ide*, 2010; *Rubin*, 2011]. This study presents high-resolution simulations that reproduce many of the observed space-time characteristics of SSEs.

The simulations use an idealized subduction zone configuration, where the mega-thrust is divided into three sections based on sliding characteristics: a seismogenic zone, a transition zone (where SSEs occur), and a creeping zone (Figure 4.1). The rate- and state-dependent formulation is employed to represent constitutive properties of the mega-thrust interface. This formulation is based on laboratory observations and has found widespread use in modeling different modes of slip including earthquakes, slow slip, and continuous creep [*Dieterich,* 1979; 1981; *Ruina*, 1983]:

$$\tau = \sigma\left[\mu_0 + a\ln\left(\frac{\dot{\delta}}{\dot{\delta}^*}\right) + b\ln\left(\frac{\theta\dot{\delta}^*}{D_c}\right)\right] \tag{4.1}$$

where τ and σ are the shear and normal stress, respectively; μ_0 , *a*, and *b* are experimentally determined constants; $\dot{\delta}$ is sliding speed; $\dot{\delta}^*$ is a normalizing constant; θ is a state variable that evolves with time, slip, and normal stress history; and D_c is the characteristic sliding distance over which state evolves. See Chapter 2 for more details. The seismogenic zone is modeled as rate-weakening: $b > a$, where steady-state fault strength decreases with increasing slip speed and enables unstable earthquake slip. Because this study focuses on the time between great mega-thrust earthquakes, the seismogenic zone does not slip in these particular simulations. In contrast, the creeping zone is modeled as rate-strengthening: $b < a$ (b = 0.008; a = 0.010), where the fault slides stably at rates determined by the current stress levels. The transition zone is modeled as rate-weakening with a gradient in *b* (b = 0.011-0.013; a = 0.010) such that it is nearly rate-neutral ($b = a$) at its lower edge. Both the transition and creeping zones are assigned low effective normal stress, 4 MPa, consistent with thermal modeling [*Peacock et al.*, 2002] and seismological observations [*Kodiara et al.*, 2004].

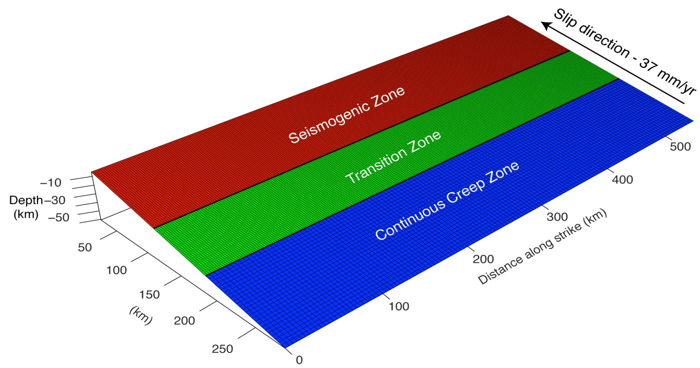

Figure 4.1. *Fault model used in this study. The seismogenic zone (red), the section of the mega-thrust that generates great earthquakes, is located between depths of 5 km and 25 km. The transition zone (blue) is located at depths of 25 km and 40 km. The creeping zone (green) is located at depths >40 km. Slip on the fault is pure-thrust with a convergence rate of 37mm/yr. The fault is 552 km x 286 km and dips 12°. Fault elements are 2 km x 2 km in the seismogenic and transition zones (red and green, respectively) and 4 km x 4 km in the continuous creep zone (blue). Total number of fault elements is 26,634.*

We employ the simulation code, Rate-State-Quake-Simulator, RSQSim, to model the various sliding behaviors and to investigate how slip propagates during SSEs. See Chapter 2 for more details. The code fully incorporates 3D stress interactions, which includes the effects of normal stress fluctuations on sliding friction, and incorporates rate- and state-dependent frictional properties. RSQSim has been used to model strike-slip faults with complex geometries [*Dieterich and Richards-Dinger*, 2010] and SSEs along a Cascadia-like mega-thrust [*Colella et al.*, 2011]. The simulations of earthquakes and SSEs utilize analytic solutions for spontaneous nucleation of events [*Dieterich*, 1992; *Fang et al.*, 2010], and event-driven computational steps as opposed to time stepping at closely spaced intervals, for computational efficiency. SSEs are modeled as slow earthquakes, wherein the slip speed during a SSE is specified as an input parameter based on observations (10^{-6} m/s), rather than an outcome of the calculations. Otherwise simulations are fully deterministic in nucleation, propagation speed, extent of slip, and final distribution of slip.

Results reported here are from simulations with ~200,000 SSEs that occur over ~200 years with equivalent moment magnitudes that range from ~M_w4.0 to ~M_w7.0. Characteristics of simulated SSEs, which include inter-event times, average slips, and durations, are consistent with characteristics of observed SSEs in Cascadia and Nankai (Figure 4.2).

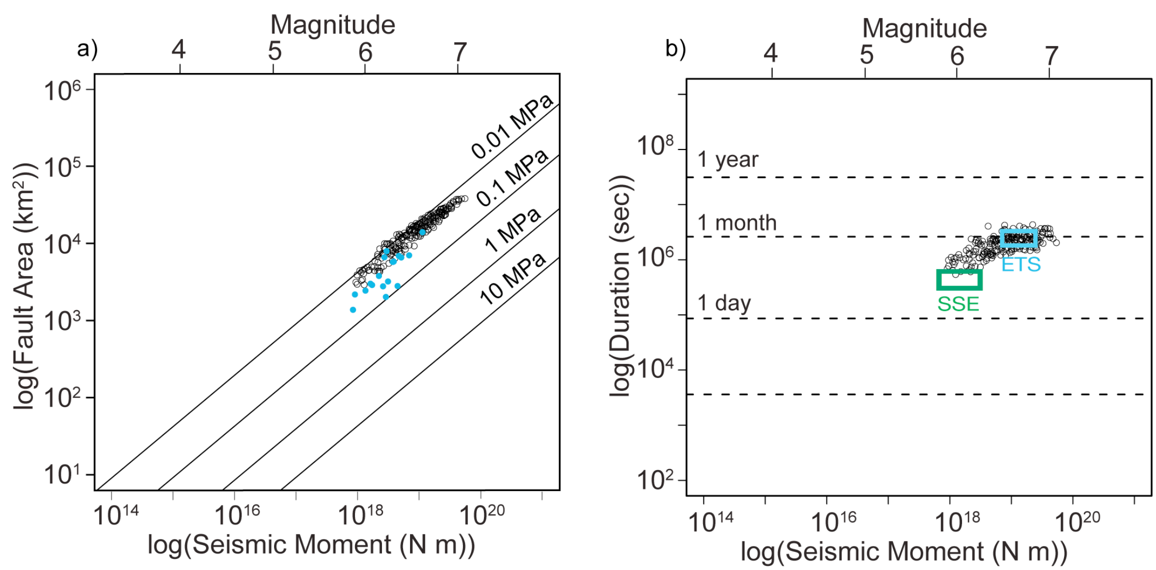

Figure 4.2: *Open black circles represent equivalent M_w>5.9 SSEs from the simulation. a) Seismic moment versus fault area in the transition zone (excluding slip in creeping zone). Light blue dots represent SSEs from Cascadia* [*Schmidt and Gao*, 2010]. *Diagonal lines contour constant static stress drop for a circular crack. b) Seismic moment versus duration. Blue and green rectangles are SSEs reported for Cascadia and Nankai, respectively* [*Ide et al.,* 2007].

Simulated SSEs exhibit complex patterns similar to observed tremor patterns [*Shelly et al.*, 2007; *Kao et al.*, 2009; *Boyarko and Brudzinski,* 2010; *Ghosh et al.*, 2010; 2011; *Ide,*, 2010; *Houston et al.*, 2011; *Wech and Creager*, 2011] (Figure 4.3). 1) Slip often initiates near the base of the transition zone [*Wech and Creager*, 2011] (Figure 4.3., right panels). 2) High background rates of very small SSEs, particularly near the base of the transition zone, may correspond to low-level background tremor [*Wech and Creager*, 2011]. 3) Incoherent slip typically occurs for several days before developing into a coherent rupture front, similar to behavior seen in tremor studies [*Houston et al.*, 2011] (Figure 4.3). 4) Different regions often slip simultaneously, which results in overlapping rupture times (Figure 4.3, left panels), referred to as “jumping” in some tremor studies [*Boyarko and Brudzinski*, 2010; *Obara*, 2010]. 5) Slip propagates along strike in a variety of ways, which includes unilateral (Figure 4.3a) and bilateral propagation (Figure 4.3c) and bilateral convergence, where slip initiates in discontinuous locations and then coalesces [*Boyarko and Brudzinski*, 2010] (Figure 4.3e & 4.3g). 6) Rupture propagation speeds often vary along strike for an individual SSE [*Ghosh et al.*, 2011]. 7). Incoherent slip occurs for several days at the end of an event, similar to tremor studies [*Houston et al.*, 2011]. 8) As previously mentioned [*Colella et al.*, 2011], back-propagating pulses across previously slipped regions propagate faster than the main front (Figure 4.3), similar to rapid tremor reversals [*Houston et al.*, 2011]. 9). Rapid along-dip slip appears in SSE simulations (Figure 4.3, right panels), similar to reported along-dip tremor streaks [*Shelly et al.*, 2007; *Ghosh et al.,* 2010; 2011].

These patterns of observed and simulated SSEs are significantly different and more complex than those of earthquake slip events. Based on the simulations, the complexity of SSEs appears to develop primarily as a consequence of the high rates of occurrence of SSEs combined with very long event durations. Together, these characteristics mean that simultaneous slip at scattered locations frequently occurs. In turn, initially independently slipping regions may interact and coalesce (e.g. bilateral convergence). The high background rates of SSEs are a consequence of low stress drops

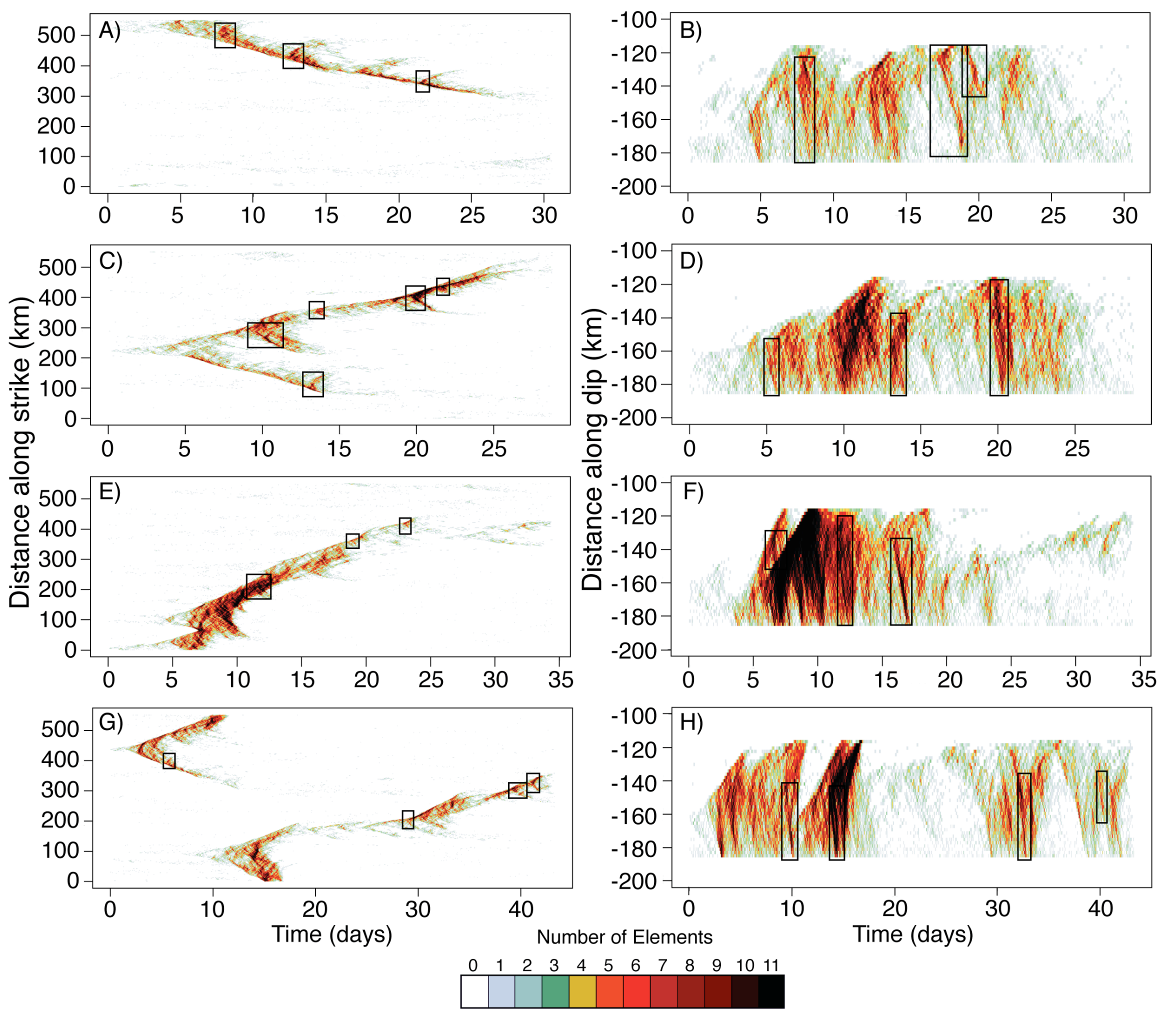

Figure 4.3. *Space-time evolution of slip during simulated SSEs. Colors correspond to the number of patches along-strike or along-dip (left and right panels, respectively) that slip at a given time. Note the high background rate of scattered very small slip events. A). Example of unilateral propagation. B). Along-dip evolution of slip from SSE in A). C) Example of bilateral propagation. D). Along-dip evolution of slip from SSE in C). E) Example of bilateral convergence. F). Along-dip evolution of slip from SSE in E). G). Example of an SSE where slip occurs at non-contiguous locations, where the region of slip eventually overlap. H). Along-dip evolution of slip from SSE in G). Black rectangles highlight back propagation pulses.*

(0.01–0.1MPa for simulated SSEs compared to typical stress drops in earthquakes of 1–10MPa). The very long event durations are a consequence of very slow slip speeds (1 µm/sec for simulated SSEs compared to slip speeds of ~1m/sec for earthquakes) and low propagation speeds.

Propagation speeds for larger simulated SSEs, $M_w \geq 6.3$ are shown in Fig. 3. Forward propagation speeds range from 9-22 km/day (Figure 4.4a). Along-strike back propagation speeds range from 30-140 km/day (Figure 4.4b). Along-dip propagation speeds range from 20-270 km/day (Figure 4.4c). The forward propagation speeds in the simulations are consistent with analytical solutions [*Colella et al.*, in review]. Those

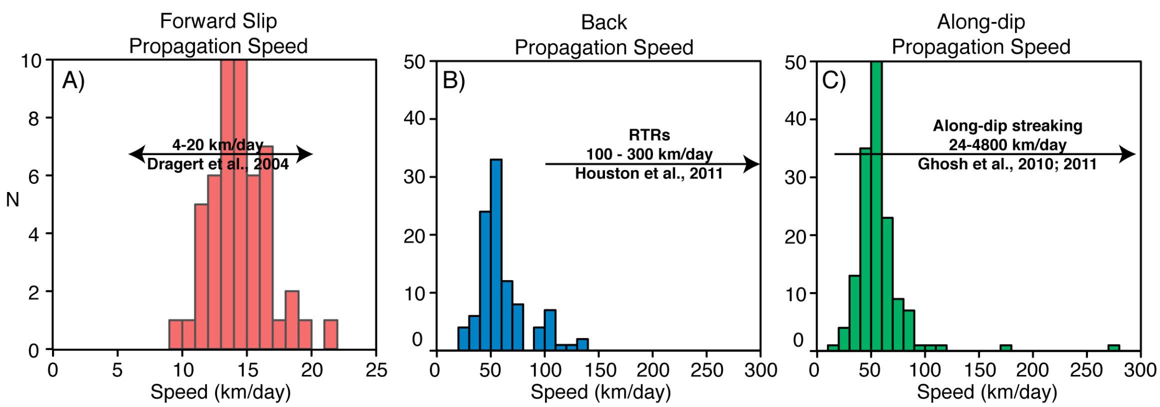

Figure 4.4. *Distribution of propagation speeds for simulated SSEs. a). Forward propagation speeds, where speeds represent the average of 2-day average speeds for all events with >6 days of coherent propagation. b). Back Propagation. c). Slip-parallel propagation.*

solutions show the propagation speed is proportional to the imposed slip speed, but is otherwise relatively insensitive, at least within the range of parameters adopted here, to parameters such as grid spacing that do not appear in standard continuum models of rate-and-state friction. The same solutions indicate that back propagation speeds should be

~4x faster than the main front, which is in agreement with simulated speeds. Observations of rapid tremor reversals suggest back propagation speeds of ~10-30x faster than forward propagation speeds; one possible explanation for this difference from the simulations is that the slip speed in the simulations is held at a fixed value, while in back-propagating pulses it may be 2-8x higher than at the main front.

In the simulations, the more rapid speed of back propagation is a consequence of time-dependent frictional healing after termination of slip behind the main rupture front, a characteristic feature of rate-state friction (Figure 5). For renewed slip to occur, the stress at the rupture front must rise to surmount the strength of the interface, which is

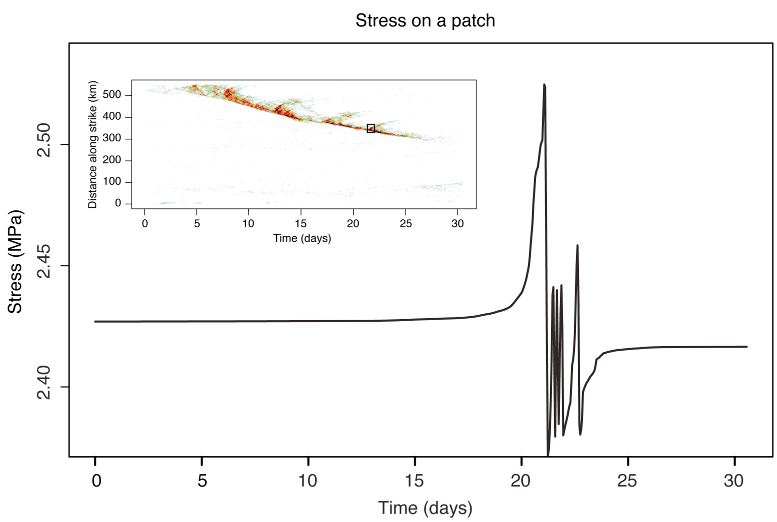

Figure 4.5. *Stress as a function of time for an element involved in the backward propagation pulse shown in inset. Inset is the event shown in Fig. 4.3a.*

dependent on the time a patch has had to heal since last slipping. For the main rupture front, which propagates across an area of the interface that has not slipped since the last SSE, this time will be on the order of a year, compared to minutes to hours for reactivated slip in backward or along-dip propagating fronts. Because the stressing rate at the rupture front is primarily controlled by slip speed, which is fixed, a lower stress barrier for reactivated slip means it can propagate at much faster speeds. However, because an element heals as the logarithm of elapsed time, it seems difficult to account for the full range of observed propagation speeds by this mechanism alone. A specific prediction of this mechanism, which can be tested against future observations, is that back propagation speeds are fastest immediately behind the main rupture front and decrease as the back-propagating front encounters parts of the fault that have had more time to heal since slipping during passage of the main front.

In summary, this is the first modeling technique that has reproduced high-resolution characteristics of observed SSEs, which include slow, incoherent initiation, complex slip patterns during events, and more rapid back propagation, over 100s of cycles. To achieve back- and along-dip propagation speeds as rapid as those observed, non-uniform slip speeds, heterogeneity, or more complicated friction laws [*Rubin*, 2011] might be required. Reports of extremely high slip-parallel propagation speeds could also represent apparent speeds that result when the main front obliquely encounters dip-parallel streaks with enhanced capability to generate tremor. Such conditions will be modeled in the future. Additionally, RSQSim will be employed to explore the effects SSEs have on the up-dip, seismogenic zone of the mega-thrust, which is responsible for world's largest earthquakes.

4.1 References:

Aguiar, A. C., T. I. Melbourne, and C. W. Scrivner (2009), Moment release of Cascadia tremor constrained by GPS, *J. Geophys. Res.*, **114**, B00A05, doi:10.1029/2008JB005909.

Ando, R., R. Nakata, and T. Hori, A slip pulse model with fault heterogeneity for low-frequency earthquakes and tremor along plate interfaces, *Geophys. Res. Lett.*, *37,* L10310, doi:10.1029/2008GL043056.

Boyarko, D. C., and M. R. Brudzinski (2010), Spatial and temporal patterns of nonvolcanic tremor along the southern Cascadia subduction zone. *J. Geophys. Res., 115*, B00A22, doi:10.1029/2008JB006064.

Colella, H. V., J. H. Dieterich, and K. B. Richards-Dinger (2011), Multi-event simulation of slow slip events for a Cascadia-type subduction zone, *Geophys. Res. Lett*., *38*, L16312, doi:10.1029/2011GL048817.

Colella, H. V., J. H. Dieterich, K. B. Richards-Dinger, and A. Rubin, Complex characteristics of slow slip events reproduced in multi-cycle simulations, *submitted.*

Dieterich, J. H. (1979), Modeling of rock friction 1. Experimental results and constitutive equations, *J. Geophys. Res.,* **84**, 2161-2168.

Dieterich, J. H. (1981), Constitutive properities of faults with simulated gouge, in Monograph 24, Mechanical behavior of crustal rocks, edited by N. L. Carter, M. Friedman, J. M. Logan, and D. W. Sterns, Am. Geophys. Union, Washington, D. C., 103-120.

Dieterich, J. H., and K. Richards-Dinger (2010), Earthquake recurrence in simulated fault systems, *Pure Appl. Geophys.,* doi:10.1007/s00024-010-0094-0.

Dragert, H., K. Wang, and T. S. James (2001), A silent slip event on the deeper Cascadia subduction interface, *Science, 292*, 1525-1528.

Ghosh, A., J. E. Vidale, J. R. Sweet, K. C. Creager, A. G. Wech, H. Houston, and E. E. Brodsky (2010), Rapid, continuous streaking of tremor in Cascadia, *Geochem. Geophys. Geosyst.*, *11*, Q12010, doi:10.1029/2010GC003305.

Ghosh, A., J. E. Vidale, and K. C. Creager (2011), paper presented at the Annual Seismological Society of America, Memphis, TN, 13-15 April.

Houston, H., B. G. Delbridge, A. G. Wech, and K. C. Creager (2011), Rapid tremor reversals in Cascadia generated by a weakened plate interface, *Nature Geosci.*, *4*, 404-409, doi:10.1038/ngeo1157.

Ide, S. (2010), Striations, duration, migration and tidal response in deep tremor, *Nature*, *466,* 356-359, doi:10.1028/nature09251.

Ide, S., G. C. Beroza, and D. R. Shelly (2007), T. Uchide, A scaling law for slow earthquakes, *Nature*, *447,* 76-79, doi:10.1038/nature05780.

Kao, H., S-J. Shan, H. Dragert, and G. Rogers (2009), Northern Cascadia episodic tremor and slip: A decade of observations from 1997 to 2007, *J. Geophys. Res., 114*, B00A12, doi:10.1029/2008JB006046.

Kodaira, S., T. Iidaka, A. Kato, J.-O. Park, T. Iwasaki, and Y. Kaneda (2004), High pore fluid pressure may cause silent slip in the Nankai trough, *Science, 304*, 1295-1298, doi: 10.1126/science.1096535.

Miller, M. M., T. Melbourne, D. J. Johnson, and W. Q. Sumner (2002), Periodic slow earthquakes from the Cascadia subduction zone, *Science*, *295*, 2423.

Obara, K. (2010), Phenomenology of deep slow earthquake family in southwest Japan: spatiotemporal characteristics and segmentation, *J. Geophys. Res.*, *115*, B00A25, doi: 10.1029/2008JB006048.

Obara, K., H. Hirose, F. Yamamizu, and K. Kasahara (2004), Episodic slow slip events accompanied by non-volcanic tremors in southwest Japan subduction zone, *Geophys. Res. Lett., 31*, L23602, doi:10.1029/2004GL020848.

Peacock, S. M., K. Wang, and A. M. McMahon (2002), Thermal structure and metamorphism of subducting oceanic crust: Insight into Cascadia intraslab earthquakes, in *The Cascadia Subduction Zone and Related Subduction Systems: Seismic Structure, Intraslab Earthquakes and Processes, and Earthquake Hazards*, edited by S. Kirby, K. Wang, and S. Dunlop, *U.S. Geol. Surv. Open File Rep.*, *02-328*, 123-126.

Rubin, A. M. (2011), Designer friction laws for bimodal slow slip propagation speeds. *Geochem. Geophys. Geosyst.*, *12*, Q04007, doi:10.1029/2010GC003386.

Ruina, A. (1983), Slip instability and state variable friction laws, *J. Geophys. Res., 88*(B12), 10359-10370.

Schmidt, D. A., and H. Gao (2010), Source parameters and time-dependent slip distribution of slow slip events on the Cascadia subduction zone from 1998 to 2008, *J. Geophys. Res., 115*, B00A18, doi:10.1029/2008JB006045.

Schwartz, S. Y, and J. M. Rokosky (2007), Slow slip events and seismic tremor at circum-Pacific subduction zones, *Rev. of Geophys., 45*, RG3004/2007.

Shelly, D. R., G. C. Beroza, and S. Ide (2007), Complex evolution of transient slip derived from precise tremor locations in western Shikoku, Japan, *Geochem. Geophys. Geosyst., 8*, Q10014, doi:10.1029/2007GC001640.

Wech, A. G., and K. C. Creager (2011), A continuum of stress, strength and slip in the Cascadia subduction zone, *Nature Geosci.*, *4,* doi:10.1038/ngeo1215.

Chapter 5

Depth-dependent characteristics of simulated slow slip events

5.1 Introduction

Since the discovery of slow slip events (SSEs) it has become apparent that a variety of slip modes exist along a subduction zone megathrust. At shallow depths (<25 km) the megathrust slips infrequently in great earthquakes with large displacements. At depths of 25-45 km the megathrust regularly slips in SSEs with small displacements. At greater depths (>45 km) the megathrust stably slides to accommodate convergence. *Wech and Creager* [2011] recently presented a conceptual model of subduction zone dynamics (hereinafter referred to as the "Wech-Creager model") that suggests a continuum of slip frequency and size from less frequent, larger slip events at shallower depths to more frequent, smaller slip events at deeper depths along the megathrust (Figure 5.1). They postulate this behavior is a consequence of the fault weakening with depth and continuous stress transfer from the creeping zone at depth. However, few observations are currently available to support or refute their model. Additionally, little attention has been paid to SSEs and tremor during the inter-SSE period. Detection limitations of small SSEs and deep events also presents difficulties when attempting to quantify how SSE characteristics vary with depth.

In this study I employ RSQSim to develop a physical basis for the Wech-Creager model of the subduction zone megathrust that gives rise to depth-dependent characteristics of SSEs, including frequency of slip events, displacement during events, and stresses. It is also my goal to quantify cumulative displacements along-dip within the transition zone. In addition, I explore the effects of varying the constitutive properties in the transition zone to determine the sensitivity of the frequency and displacements of slip events with depth to different frictional characteristics within the transition zone. These simulations support the Wech-Creager model, wherein convergence is accommodated through a continuum of slip, stress, and strength behaviors. The results also indicate a slip deficit in the transition zone, which may affect the downdip rupture extent of the next great earthquake and, therefore, seismic hazards for coastal cities near subduction zones. Finally, the distribution of slip in large, simulated SSEs suggests that the cumulative number of tremor swarm epicenters during SSEs could potentially be used as a proxy for the amount of slip during events.

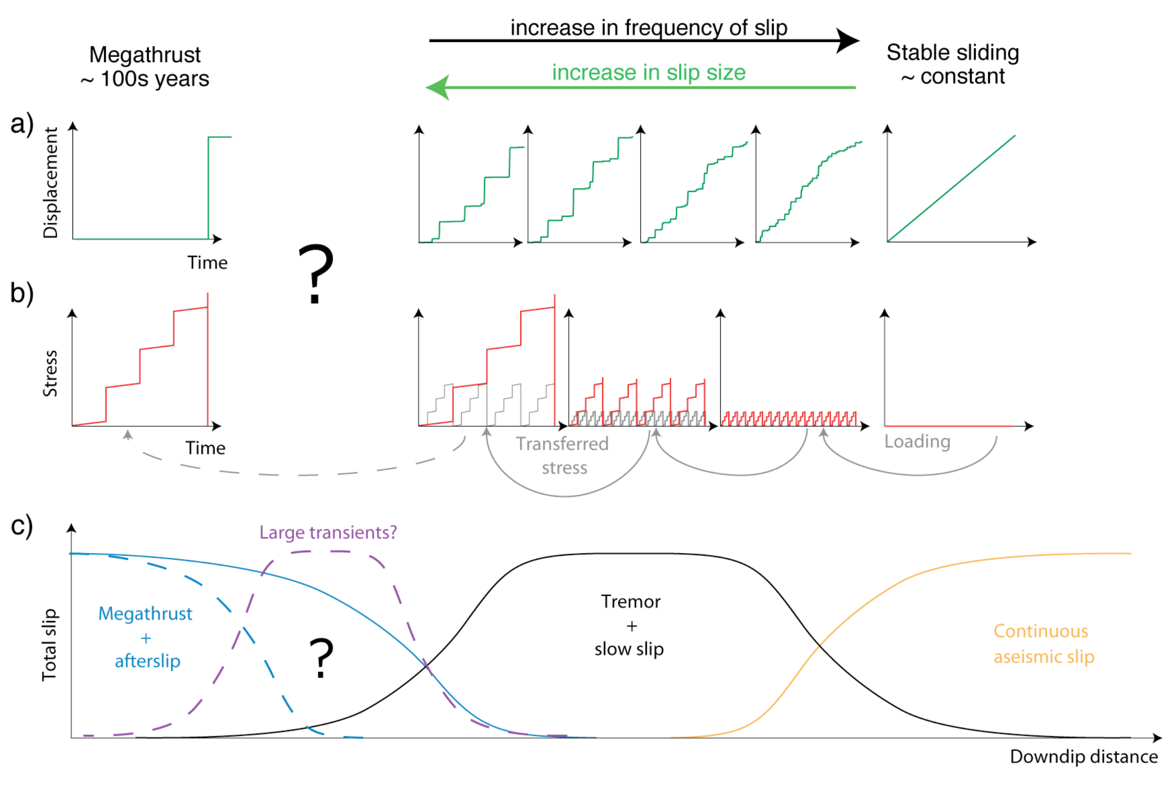

Figure 5.1. Conceptual model of subduction zone dynamics. a) *A schematic profile of displacement through time along the megathrust.* ***b)*** *A schematic profile of stress through time along the megathrust.* ***c)*** *A schematic profile of how the plate convergence is accommodated in the different regions of the megathrust (modified from Wech and Creager, 2011).*

5.2 Models

The fault model used in these simulations is similar to the fault model in Chapter 4, where the mega-thrust is divided into three sections based on sliding characteristics: seismogenic zone, transition zone (where SSEs occur), and creeping zone (Figure 5.2). The seismogenic and transition zones are modeled as rate-weakening; however, for purposes of this study the seismogenic zone does not experience slip. In contrast, the creeping zone is modeled as rate-strengthening. The transition and creeping zones are assigned a low effective normal stress (σ), 4 MPa, which implies high pore-fluid pressures, consistent with thermal modeling [*Peacock et al.*, 2002] and seismological observations [*Kodiara et al.*, 2004; *Shelly et al.*, 2006]. These conditions remain constant for all simulations presented in this chapter.

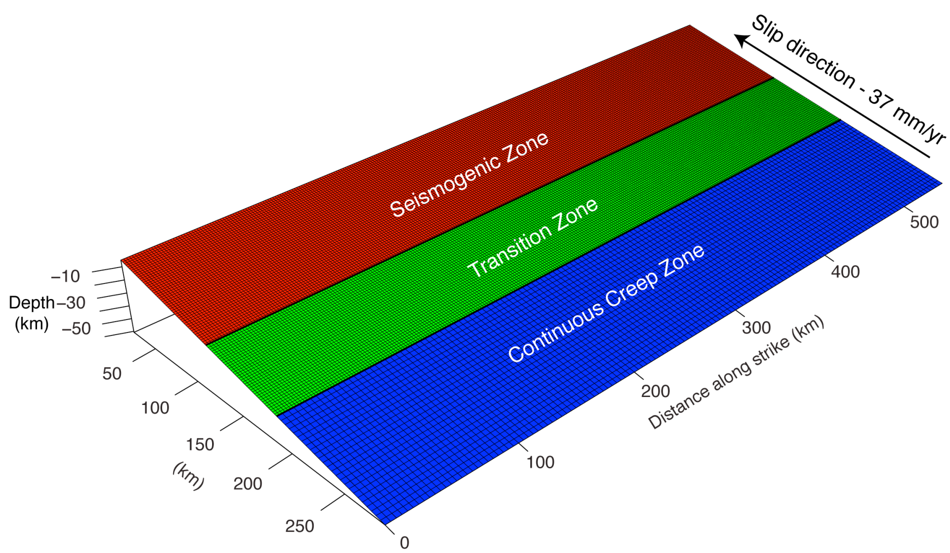

Figure 5.2: Fault model. *This fault model is the same as was used in Chapter 4. The seismogenic zone, the section of the mega-thrust that generates great earthquakes, is located between depths of 5 and 25 km. The transition zone is located at depths of 25 km and 45 km. The creeping zone is located at depths > 45 km. Slip on the fault is pure-thrust with a convergence rate of 37 mm/yr. The fault is 552 km x 286 km and dips 12°. Fault elements are 2 km x 2 km in the seismogenic and transition zones (red and green, respectively) and 4 km x 4 km in the continuous creep zone (blue). Total number of fault elements is 26,634.*

Four different models are investigated to explore the sensitivity of the frequency of slip and slip per event to the constitutive properties. While the transition zone is assigned rate-weakening conditions for all models in this study, the values of the constitutive properties within the zone vary for each model (Table 5.1). Model #1 has uniform frictional characteristics throughout the transition zone. Model #2 and #3 have a gradient in frictional characteristics, where *b* varies from values greater than *a* to nearly rate-neutral conditions ($b = a$). Model #3 has a slightly large range in *b* values. Model #4 also has a similar gradient in *a* and *b*, but with smaller absolute values. In all the models there is a step from rate-weakening in the transition zone to rate-strengthening in the creeping zone.

Table 5.1: Constitutive properties of the models in this study

	Transition Zone		**Creeping Zone**	
Model #	**a**	**b**	**a**	**b**
1	0.01	0.012	0.01	0.008
2	0.01	0.011-0.013	0.01	0.008
3	0.01	0.0105-0.0135	0.01	0.008
4	0.008	0.009-0.011	0.008	0.006

5.3 Results

Characteristics of the largest simulated SSEs ($M_w \geq 6.3$), which include inter-event times, durations, and average slips, are consistent with characteristics of observed SSEs in Cascadia (Table 5.2). For each of the four models the simulations span ~300 years, where 200,000 - 700,000 SSEs occurred in the transition zone and no earthquakes are permitted to occur in the seismogenic zone. SSEs in all simulations have moment magnitude equivalents of M_w4.0 - M_w7.0.

Table 5.2: Summary of the results from simulated SSEs M_w>6.3 compared with observations in Cascadia

	Inter-event Times	Duration	Mean Slip
Cascadia	9-22 months*	10-30 days*	2-4 cm*
Model #1	~10 months	~19 days	1.5-3.7 cm
Model #2	~11 months	~26 days	1.3-4.7 cm
Model #3	~12 months	~26 days	1.1-4.0 cm
Model #4	~10 months	~21 days	1.2-4.3 cm

*Results from *Dragert et al.* [2004]

5.3.1 Results from Model #2

A persistent feature of the all simulations is the increased frequency of slip events with increasing depth. I chose to show detailed results from Model #2 because it is the same model used in Chapter 3. Fault elements near the base of the transition zone (~40 km) slip approximately every 1-2 months, while fault elements at the updip edge of the transition zone (~25 km) slip approximately every 1-3 years. Figure 5.3b illustrates there is more variation in frequency of slip events near the base of the transition zone, which is likely related to the quiescence period that follows the largest SSEs. Figure 5.4 is a space-time plot of SSEs along-dip, which clearly shows a period of quiescence immediately following the largest SSEs ($M_w \geq 6.3$). Following the quiescence, SSEs gradually increase in size and the region of slip in each event progressively expands updip. This process culminates in a large SSE that spans the width of the transition zone. Similar trends are reported for tremor swarms in Cascadia [*Wech et al.*, 2010; *Wech and Creager*, 2011].

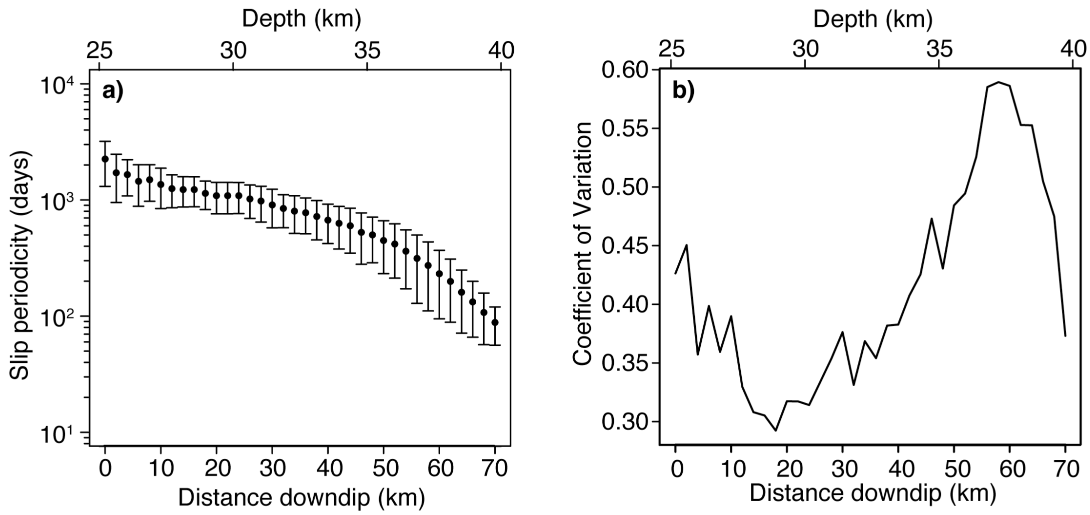

Figure 5.3: Slip periodicity. a) *The average time, in days, between slip events occurring on patches along a cross-section of the fault at 275 km along-strike for Model #2. Bars represent one standard deviation of the inter-event times.* ***b)*** *Coefficient of variation of the inter-event times. 0 km represents the updip edge of the transition zone, adjacent to the seismogenic zone.*

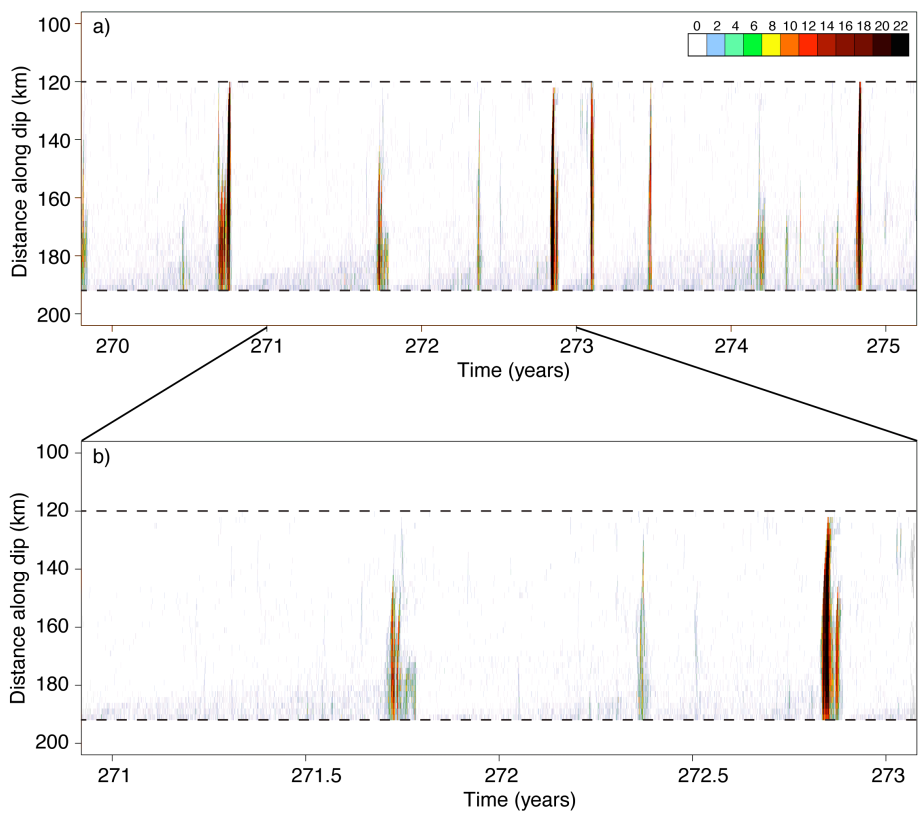

Figure 5.4: Space-time plot of SSEs. a) *Space-time evolution of slip along-dip for a 5-year period from Model #2.* ***b)*** *Expanded plot of an interval in* ***a****. Each vertical line represents a slip event. The colors correspond to the number of patches slipping simultaneously in 2 km along-strike bins. Dashed lines indicate the boundaries of the transition zone.*

In the simulations the slip per event also varies with depth along the transition zone (Figure 5.5). Note the left axis (displacement) is different for each plot, while the right axis (stress) and x-axis (time) remain the same. The time interval (265-285 years) was chosen because it is ~1/2 of the recurrence interval of the seismogenic zone, which is potentially similar to the current state of the Cascadia subduction zone. The curves illustrate displacement and stress on a single patch at 4 depths (red and black curves,

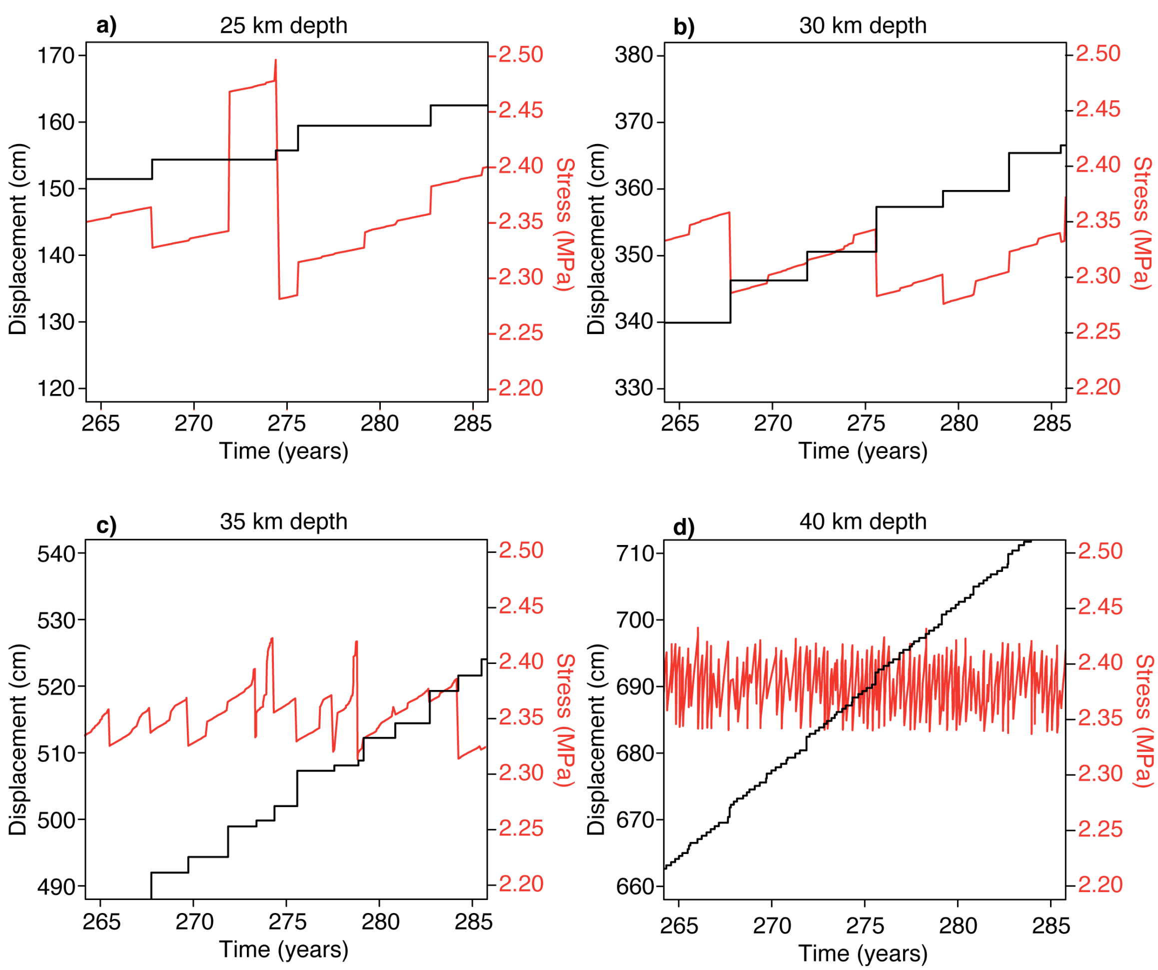

Figure 5.5: Displacement and stress with depth. a) *25 km.* ***b)*** *30 km.* ***c)*** *35 km.* ***d)*** *40 km at 275 km along strike. Black curve represents displacement and red curve represents stress for Model #2.*

respectively), where each step in displacement indicates a SSE. The base of the transition zone experiences frequent SSEs, approximately every 1-2 months, with displacements of < 1 cm per event (Figure 5.5d), while the updip edge of the transition zone, adjacent to the seismogenic zone, experiences occasional SSEs, approximately every 1-3 years, with displacements of ~1-3 cm per event (Figure 5.5a). Consequently, ~6x more displacement occurs near the base of the transition zone (~40 km) compared to updip edge (~25 km). Notice the largest displacements per event occur at ~30-35 km depth. Figure 5.5 also shows that stress at every depth fluctuates around the shear strength of the fault (~2.4 MPa). However, because of continuous slip in the creeping zone, the base of the transition zone is more rapidly loaded, which results in rapid accumulation and release of stress. With decreasing depth, stress slowly increases from continual loading and the occurrence of SSEs downdip until the frictional strength is overcome.

5.3.2 Sensitivity to assigned constitutive properties

Four models are explored to understand the sensitivity of the results to the constitutive properties. Figure 5.6 and Figure 5.7 compare the frequency of slip events with depth and displacement at 4 locations, respectively, for 4 models with different constitutive properties in the transition zone. In Model #3, where (b - a) is the smallest along the base of the transition zone (*0.0005*), slip occurs much more frequently with depth than in the other models (Figure 5.6, purple circles). Because slip occurs more frequently, the slip per event is also much smaller (Figure 5.7d, purple curves). Conversely, in Model #1, where (b - a) is largest along the base of the transition zone

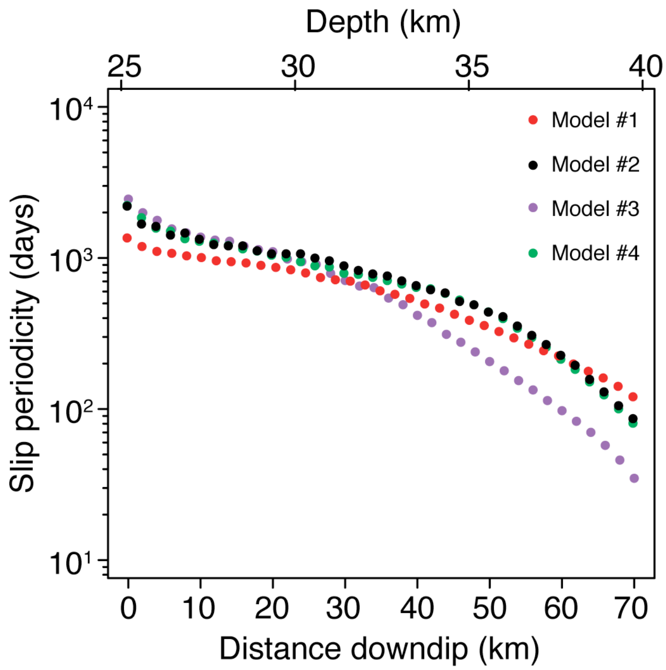

Figure 5.6. Slip periodicity with depth. *Results for the 4 models explored in this study. 0 km represents the boundary between the transition zone and the seismogenic zone.*

(*0.002*), slip occurs less frequently with depth than in the other models (Figure 5.6, red circle). For Model #2 and Model #4, where the gradient of (*b* - *a*) is the same but the values for *a* and *b* are different, the model with the smaller *a* and *b* values (Model #4, green circles) has more frequent slip with depth. Model #1, which has uniform constitutive properties, has more frequent slip at the updip edge of the transition zone because (*b* - *a*), which controls the stress drop and hence slip, is smallest at this depth interval in this model. These results indicate the constitutive properties chosen can have a significant effect on the frequency of slip and cumulative displacement with depth in the transition zone.

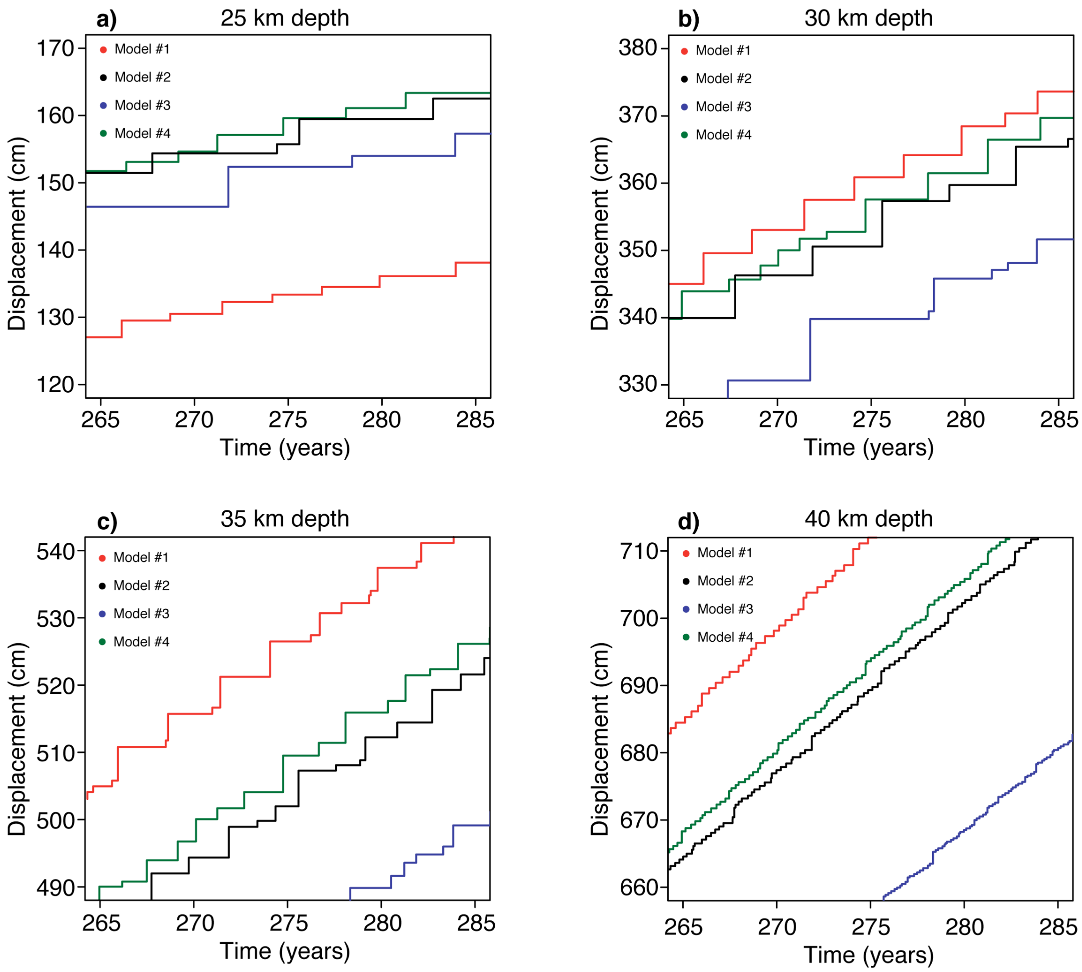

Figure 5.7. Displacement with depth. *Results from the 4 models explored in this study at 4 depths located 275 km along strike. a). 25 km depth. b). 30 km depth. c). 35 km depth. d). 40 km depth.*

5.4 Discussion

Many of the results of the simulations support the Wech-Creager model. The simulations produce a range of slip behaviors from continuous creep at depth to small, frequent SSEs with small displacements near the base of the transition zone to larger, less frequent SSEs with larger displacements as the depth along the transition zone decreases (Figure 5.3 and 5.4). The largest SSEs ($M_w \geq 6.3$) are followed by a period of quiescence throughout the entire transition zone. As SSEs increase in size, the region of slip progressively expands updip, culminating in a large SSE. Similar depth-dependent characteristics are observed in tremor swarms epicenters from *Wech and Creager* [2011], where the frequency of tremor swarm occurrence, or slip, increases with horizontal distance downdip. *Wech and Creager* [2011] commonly use tremor epicenters in terms of horizontal, downdip distance from a reference line at the updip edge of the 95% of all tremor swarms because of large depth uncertainties and discrepancies between different models of the plate interface. Stress accumulation (and release) also has depth-dependent characteristics, wherein stress transfer from the creeping zone to the transition zone results in the most rapid stress accumulation at the base of the transition zone (Figure 5.5d). Hence, recovery of SSE activity following the period of quiescence is driven by frequent slip events at the base of the transition zone that progressively transfer stress updip. The high frequency of SSEs at the base of the transition zone is the result of continual loading from the creeping zone at depth, which supports the hypothesis presented by *Wech and Creager* [2011].

A possible departure of simulated displacements within the transition zone compared to the model of displacements (Figure 5.1a) proposed by *Wech and Creager* [2011] is that the largest displacements per event does not occur at the top of the transition zone. The largest displacements in the simulations occur near the center of the transition zone. This is a result of a locked seismogenic zone, which may be more representative of a Cascadia-like subduction zone, in that little to no activity (earthquake slip or slow slip) is currently observed in this region. Instead the Wech-Creager model is based on the possibility of long-term SSEs (see Chapter 1 for more information) in this region; however no such events have been identified in Cascadia at this time.

The simulations may provide an argument for tremor to serve not only as a proxy for the extent of slip, but also for the amount of slip. As previously noted, the maximum slip per simulated SSEs occurs near the center of the transition zone, ~35 km from the the updip edge, which coincides with peak in the number of tremor swarm epicenters

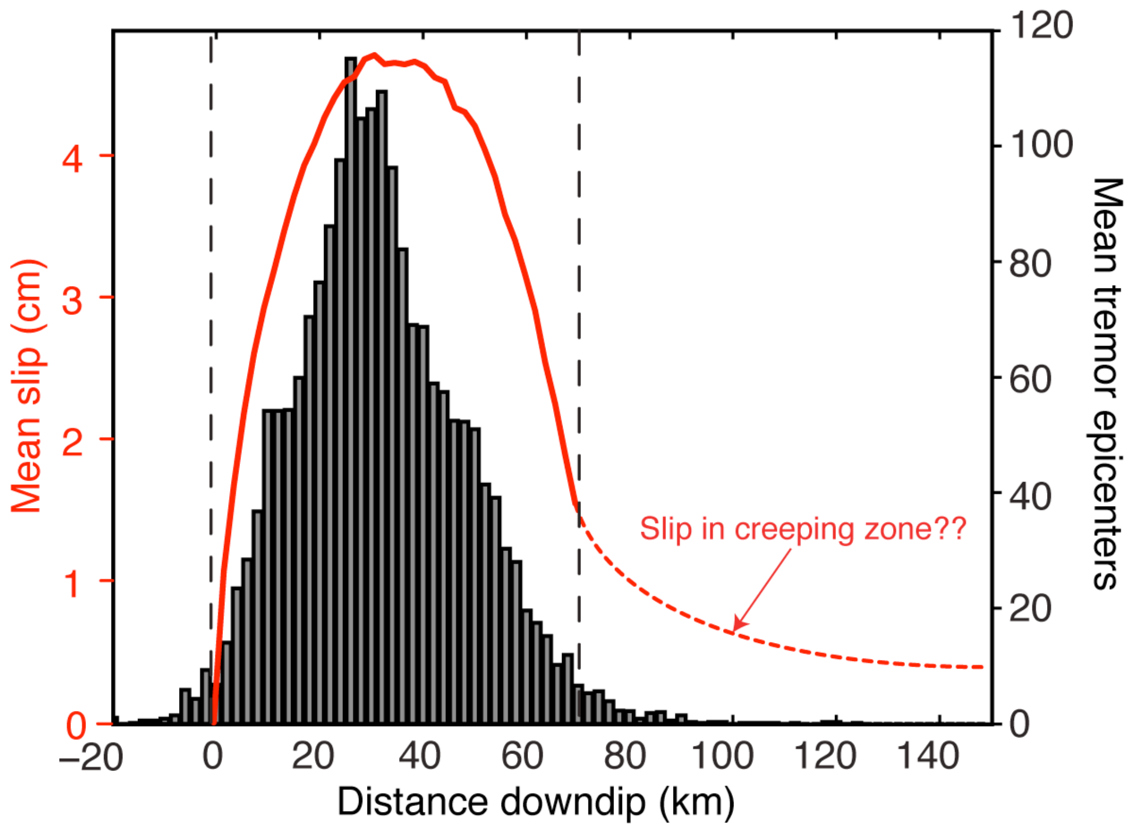

Figure 5.8. Slip and tremor comparison. *The solid red curve represents the mean slip from simulated SSEs $M_w > 6.3$ along a cross section of the transition zone at 275 km. The red dashed line represents possible slip in the creeping zone. Grey bars represent tremor epicenters along dip for 8 SSEs in Cascadia. Black dotted lines denoted the boundaries of the transition zone. (Tremor data courtesy of Aaron Wech).*

(Figure. 5.8). Figure 5.8 is a plot of the mean slip for the largest SSEs ($M_w \geq 6.3$) and the mean number of tremor swarm epicenters from SSEs in Cascadia as a function of distance along dip. Although the distribution of tremor swarm epicenters is more sharply peaked than the slip, the locations of both the peak and width of the distributions are similar. It is also possible there is a deficit in tremor swarm epicenters closer to the base of the transition zone due to detection limitations with increasing depth.

Varying the constitutive properties within the transition zone affects the frequency of slip events and the average displacement per event as a function of depth. In Models #2, #3, and #4, where the *b* parameter gets smaller with depth, slip is more frequent near the base of the transition zone compared to Model #1, where the *b* parameter is uniform (Figure 5.6). This is a result of near rate-neutral ($b \approx a$) constitutive properties along the base of the transition zone in Models #2, #3, and #4, which results in very low stress drops. Consequently, the slip per event near the base of the transition zone is smaller in these models than in Model #1 (Figure 5.7). A reduction of absolute values of *a* and *b* (Model #4, green circles), where (b - a) is the same as Model #2 (black circles), has little affect on the frequency of slip with depth. Overall, the simulations produce less frequent slip with depth, particularly at shallow depths, than reported by *Wech and Creager* [2011] for tremor observations, where they use tremor as a proxy for slip. This disparity is likely a result of the chosen model parameters. Future modeling studies will aim to more accurately replicate slip periodicity at shallow depths.

Finally, the simulations show a significant slip deficit within the transition zone after 285 years (Figure 5.9), approximately the duration since the last great Cascadia earthquake. This may have profound effects on the characteristics of earthquake occurrence in the locked zone. Simulations described in Chapter 3 show that SSEs penetrate into the creeping zone during large SSEs. Because of the low strength of the transition zone, it is possible the next great earthquake will, similarly, penetrate deep into

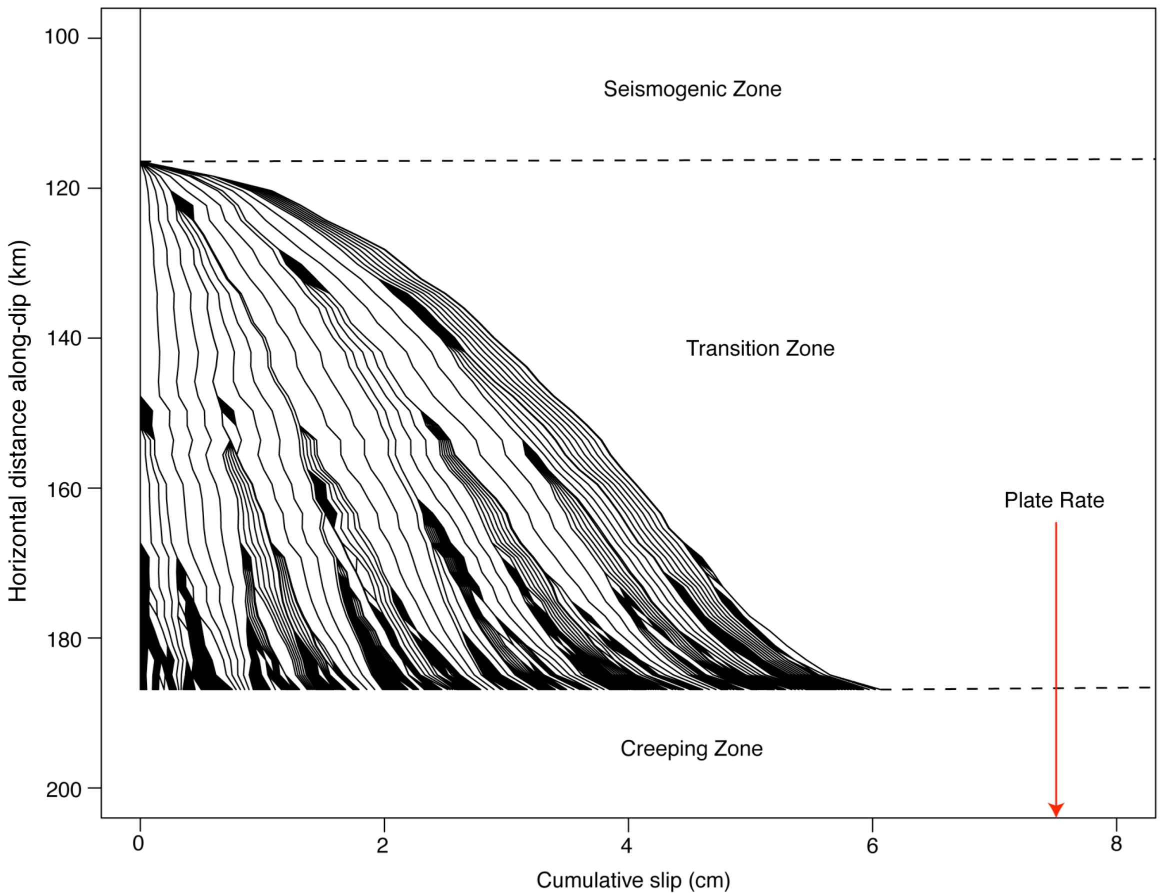

Figure 5.9. Displacement with depth. *Slip in centimeters on the horizontal axis versus the horizontal distance along-dip for 20 years (265-285 years) of SSEs (Model #2). During a SSE slip steps are shown in 3-day intervals. Between SSEs slip steps are shown in 30-day intervals*

the transition zone to recover some or all of the slip deficit. Alternatively, the slip deficit may be recovered during afterslip, as occurred following the M_w8.0 1995 Colima-Jalisco, Mexico earthquake, where afterslip occurred for 3.5 years between 16-35 km depth

[*Hutton et al.*, 2001] or the M_w8.4 2001 Peru earthquake, where 25% of the total coseismic slip was released as afterslip immediately downdip of the main rupture [*Melbourne et al.*, 2002]. The afterslip may be composed of accelerated SSEs. Future studies will focus on the interactions and feedback between the seismogenic zone and transition zone to better assess the seismic hazard for coastal communities near subduction zones.

5.5 References:

Dragert, H., K. Wang, and G. Rogers (2004), Geodetic and seismic signatures of episodic tremor and slip in the northern Cascadia subduction zone, *Earth Planets Space, 56*(12), 1143–1150.

Hutton, W., C. DeMets, O. Sanchez, G. Suarez, and J. Stock (2001), Slip kinematics and dynamics during and after the 1995 October 9 Mw = 8.0 Colima-Jalisco earthquake, Mexico, from GPS geodetic constraints, *Geophys. J. Int., 146*, 637–658.

Kodaira, S., T. Iidaka, A. Kato, J. O. Park, T. Iwasaki, Y. Kaneda (2004), High pore fluid pressure may cause silent slip in the Nankai trough, *Science, 304*, 1295-1298, doi: 10.1016/science.1096535.

Melbourne, T. I., and F. H. Webb (2002), Precursory transient slip during the 2001 Mw = 8.4 Peru earthquake sequence from continuous GPS, *Geophys. Res. Lett.*, *29*(21), 2032, doi:10.1029/ 2002GL015533.

Peacock, S. M., K. Wang, and A. M. McMahon (2002), Thermal structure and metamorphism of subducting oceanic crust: Insight into Cascadia intraslab earthquakes, in *The Cascadia Subduction Zone and Related Subduction Systems: Seismic Structure, Intraslab Earthquakes and Processes, and Earthquake Hazards*, edited by S. Kirby, K. Wang, and S. Dunlop, *U.S. Geol. Surv. Open File Rep.*, *02-328*, 123-126.

Shelly, D. R., G. C. Beroza, S. Ide, and S. Nakamula (2006), Low frequency earthquakes in Shikoku, Japan, and their relationship to episodic tremor and slip, *Nature, 442*, 188–191, doi:10.1038/nature04931.

Wech, A. G., and K. C. Creager (2011), A continuum of stress, strength and slip in the Cascadia subduction zone, *Nature Geosci.*, doi:10.1038/NGEO01215.

Wech, A. G., K. C. Creager, H. Houston., J. E. Vidale (2010), An earthquake-like magnitude-frequency distribution of slow slip in northern Cascadia, *Geophys. Res. Lett.*, *37*, L22310, doi:10.1029/2010GL04488.

Chapter 6

Conclusions

6.1 Summary

This work employs a physics-based, computationally efficient, earthquake simulations code, RSQSim, to produce 100s-1000s of cycles of SSEs along a subduction zone interface. Because this method is capable of generating long histories of SSEs (i.e. ~250,000 events over ~300 years), the characteristics and scaling relationships of SSEs can be investigated. Additionally, this study explores the interactions between SSEs and adjacent fault sections.

Chapter 3 presents initial results from multi-event simulations of SSEs. The largest simulated SSEs ($M_w > 6.3$) show the characteristics of simulated SSEs are in broad agreement with observations of SSEs in Cascadia and Nankai. Below M_w5.6 SSEs usually exhibit quite incoherent rupture growth with irregular geometries, and could be described as swarms of smaller sub-events. Simulated results also suggest the moment magnitude-duration scaling may not be linear as originally suggest by *Ide et al.*, [2007]. Finally, results show that the stressing rate on the adjacent seismogenic zone during a SSE is ~100x higher than the stressing rate during the inter-SSE period. Such conditions may favor increased seismicity along the base of the seismogenic zone and enhanced probabilities of nucleation of the next great earthquake coincident with a SSE.

The study in Chapter 4 is the first of its kind to reproduce high-resolution characteristics of observed SSEs. These include slow, incoherent initiation of SSEs near the base of the transition zone, incoherent termination of events, and rapid, renewed slip behind the main front, both parallel to and perpendicular to the direction of slip.

Simulated SSEs are shown to be quite complex and are quite different in character from earthquake slip events. SSEs frequently exhibit simultaneous slip at scattered locations because of their high rates of occurrence and long event durations. The work detailed in Chapter 4 also complements observational studies of complex tremor migration patterns coincident with SSEs [*Obara*, 2002; *Dragert et al.*, 2004; *Shelly et al.*, 2007; *Boyarko and Brudzinski*, 2010; *Ghosh et al.*, 2010; 2011; *Ide,* 2010; *Obara*, 2010; *Houston et al.*, 2011; *Wech and Creager*, 2011]. Not only do the results agree remarkably well with the observations, but they show that the rapid speed of back propagation is a consequence of time-dependent frictional healing after termination of slip behind the main rupture front.

Finally, Chapter 5 explores the depth-dependent characteristics of slip for simulated SSEs. The simulations illustrate that the frequency of slip increases with increasing depth, which is in agreement with observations of tremor swarm epicenters [*Wech and Creager*, 2011]. The simulations show frequency slip (~1-2 months) along the base of the transition zone, except for a quiescence after the largest ($M_w > 6.3$) SSEs. Following this period of quiescence, SSEs gradually increase in size and the region of slip progressively expands updip, until the width of the transition zone fails in the largest SSEs. The increasing frequency of slip events with increased depth is a consequence of a high stress concentration near the base of the transition zone from the creeping zone. Additionally, the region maximum slip during a SSE corresponds with the region of maximum cumulative tremor swarms. Such a result may indicate the density of identified tremor swarms during a single SSE could be used as a proxy for the amount of slip during the event. This would provide another method to constrain the magnitude of SSEs. The simulations also indicate a significant slip deficit immediately downdip of the seismogenic zone.

6.2 Impact of this research

The research study is important for several reasons. 1) It employs a new, innovative, physics-based modeling technique to explore the characteristics of SSEs and investigate the interactions between the different slip modes along a subduction zone interface. The simulations are in remarkable agreement with the observations, which provides confidence that the modeling method is producing reliable results. Additionally, this method allows different properties for the transition zone to be explored. Such capabilities may elucidate the properties necessary to produce the observed characteristics of SSEs. 2) Results from this study should be useful to the observational community in that some of the presented results have yet to be observed (i.e. the slow down of back propagation as the slip moves away from the rupture front). The results suggest moment-duration scaling relationship of $M_0 \propto t^{1.5\text{-}2.0}$ as opposed to $M_0 \propto t$, which was first proposed by *Ide et al.* [2007]. 3). This study may also have important implications for seismic hazard assessment along subduction zones. During large SSEs (M>6.3) the stressing rate on the seismogenic zone is increased by ~100x, which may increase the likelihood for a large/great earthquake to occur during a SSE. It is also possible that seismicity near the base of the seismogenic zone will increase as the stress accumulates between great earthquakes. The simulations also indicate a slip deficit within the transition zone, which may affect the downdip extent of the next great earthquake, and consequently have significant implications for seismic hazard assessment for cities near subduction zones.

6.3 Future Directions

The next step for this research is to address the following question: What is the probability that a SSE will be followed by a great earthquake in a specific time interval? Additionally, does the rate of occurrence of SSEs vary before or after a great earthquake? Furthermore, do SSEs affect the magnitude of great earthquakes? For example, results from this study show a significant slip deficit in the transition zone of a subduction zone interface (Chapter 5) as well as the penetration of SSEs into the creeping zone [*Colella et al.*, 2011; Chapter 3]; therefore it is possible that earthquakes will penetrate into the transition zone. If this occurs, does it have a significant effect on the probabilities of great earthquakes? RSQSim has recently been modified to accept two slip speeds (i.e. earthquake slip and slow slip) so that simulations can be run to explore the interactions between the seismogenic zone and transition zone.

I also plan to further investigate segmentation of the transition zone. While spontaneous segmentation does appear in the simulations [*Colella et al.*, 2011; Chapter 3], the recurrence of SSEs on individual segments does not persist for long periods of time in contrast to the observations compiled by *Brudzinski and Allen* [2007] for the Cascadia mega-thrust. I would like to test the hypotheses that have been suggested for segmentation, including lateral changes in rheology of the overlying continental crust

[*Brudzinski and Allen*, 2007], segmentation controlled by the subduction of seamount tracks [*Ide*, 2010], and fractures within the oceanic slab [*Obara*, 2009].

Despite the remarkable congruence between the simulations and observations in Cascadia and Nankai, preliminary results of ETS events from other subduction zones appear to show significantly different patterns. For example, in New Zealand the longest duration SSEs with the longest recurrence intervals occur at depths of >40 km and the shortest duration SSEs with the shortest recurrence intervals occur at depths of <10 km [*Wallace and Beavan*, 2010]. Similarly shallow SSEs have also been observed in Costa Rica [*Brown et al.*, 2005] and Shikoku, Japan [*Davis et al.*, 2006]. One hypothesis to explain these differences is that fundamentally different structural and/or mechanical properties (i.e. tears or asperities in the subduction slab or age of the subduction slab) control the characteristics of ETS in different subduction zones. The flexibility of the RSQSim modeling approach, where effective normal stress and frictional properties can be explored and models with complex fault geometries can be created, provides an opportunity to investigate different hypotheses that may control the variability in observed SSEs.

Finally, with the identification of SSEs on Kilauea [*Cervelli et al.*, 2002; *Brooks et al.,* 2006], I would like to investigate how magma-related, or volcanic, processes interact with earthquake, and/or tectonic, processes. Specifically, I am interested in how magmatic intrusions affect the recurrence rate of SSEs and decollement earthquakes. *Brooks et al.* [2008] suggest the 2007 Father's Day intrusion at Kilauea volcano triggered the most recent slow slip event. There is also evidence to suggest increased seismicity beneath Mount St. Helens associated with SSEs in Cascadia [*Gina Schmalzle*, personal communication]. I can investigate the probability that a SSE is, indeed, coincident with a magmatic intrusion with RSQSim by creating input files that reflect stress effects from magmatic processes on the decollement. Furthermore, I would explore the interactions between the decollement and magmatic processes at Kilauea volcano. Unraveling the mechanics of Kilauea's decollement could be key to understanding the internal processes of the volcano. This would open the door to investigations into the relationship between the decollement and Kilauea's other faults.

6.4 References

Boyarko, D. C., and M. R. Brudzinski (2010), Spatial and temporal patterns of nonvolcanic tremor along the southern Cascadia subduction zone. *J. Geophys. Res., 115*, B00A22, doi:10.1029/2008JB006064.

Brooks, B. A., J. Foster, D. Sandwell, C.J. Wolfe, P. Okubo, M. Poland, and D. Myer (2008), Magmatically triggered slow slip at Kilauea volcano, Hawaii, *Science, 321*, 1177.

Brown, K. M., M. D. Tryon, H. R. DeShon, L. M. Dorman, and S. Y. Schwartz (2005), Correlated transient fluid pulsing and seismic tremor in the Costa Rica subduction zone, *Earth Planet. Sci. Lett.*, *238*, 189–203.

Cervelli, P., P. Segall, K. Johnson, M. Lisowski, and A. Miklius (2002), Sudden aseismic fault slip on the south flank of Kilauea volcano, *Nature*, *415*, 1014-1018.

Colella, H. V., J. H. Dieterich, K. B. Richards-Dinger (2011), Multi-event simulations of slow slip events for a Cascadia-like subduction zone, *Geophys. Res. Lett., 38*, L16312, doi:10.1029/2011GL048817.

Davis, E. E., K. Becker, K. Wang, K. Obara, Y. Ito, and M. Kinoshita (2006), A discrete episode of seismic and aseismic deformation of the Nankai trough subduction zone accretionary prism and incoming Philippine Sea plate, *Earth Planet. Sci. Lett.*, *242*, 73–84.

Dragert, H., K. Wang, and G. Rogers (2004), Geodetic and seismic signatures of episodic tremor and slip in northern Cascadia subduction zone, *Earth Planets Space*, 56, 1143-1150.

Ghosh, A., J. E. Vidale, J. R. Sweet, K. C. Creager, A. G. Wech, H. Houston, and E. E. Brodsky (2010), Rapid, continuous streaking of tremor in Cascadia, *Geochem. Geophys. Geosyst.*, *11*, Q12010, doi:10.1029/2010GC003305.

Ghosh, A., J. E. Vidale, and K. C. Creager (2011), paper presented at the Annual Seismological Society of America, Memphis, TN, 13-15 April.

Houston, H., B. G. Delbridge, A. G. Wech, and K. C. Creager (2011), Rapid tremor reversals in Cascadia generated by a weakened plate interface, *Nature Geosci.*, *4*, 404-409, doi:10.1038/ngeo1157.

Ide, S. (2010), Striations, duration, migration and tidal response in deep tremor, *Nature*, *466,* 356-359, doi:10.1028/nature09251.

Ide, S., G. C. Beroza, D. R. Shelly, and T. Uchide (2007), A scaling law for slow earthquakes, *Nature*, *447,* 76-79, doi:10.1038/nature05780.

Obara, K. (2002), Nonvolcanic deep tremor associated with subduction in southwest Japan, *Science, 296*, 1679 – 1681, doi:10.1126/science.1070378.

Obara, K. (2010), Phenomenology of deep slow earthquake family in southwest Japan: spatiotemporal characteristics and segmentation, *J. Geophys. Res.*, *115*, B00A25, doi: 10.1029/2008JB006048.

Shelly, D. R., G. C. Beroza, and S. Ide (2007), Complex evolution of transient slip derived from precise tremor locations in western Shikoku, Japan, *Geochem. Geophys. Geosyst., 8*, Q10014, doi:10.1029/2007GC001640.

Wallace, L. M., and R. J. Beavan (2010), Diverse slow slip behavior at the Hikurangi subduction margin, New Zealand, *J. of Geophys. Res., 115:* B12402, doi: 10.1029/2010JB007717

Wech, A. G., and K. C. Creager (2011), A continuum of stress, strength and slip in the Cascadia subduction zone, *Nature Geosci.*, *4,* doi:10.1038/ngeo1215.